Structural and molecular determinants for the interaction of ExbB from *Serratia marcescens* and HasB, a TonB paralog.

Valérie Biou[1#], Ricardo Jorge Diogo Adaixo[2], Mohamed Chami[2], Pierre-Damien Coureux[3], Benoist Laurent[4], Véronique Yvette Ntsogo Enguéné [1*], Gisele Cardoso de Amorim[5*], Nadia Izadi-Pruneyre[5], Christian Malosse[6], Julia Chamot-Rooke[6], Henning Stahlberg[2*], Philippe Delepelaire[1#]

1: Laboratoire de Biologie Physico-Chimique des Protéines Membranaires, Université de Paris, UMR 7099 CNRS, F-75005, Paris, France.
Institut de Biologie Physico-Chimique, F-75005, Paris, France.
2: Center for Cellular Imaging and NanoAnalytics, Biozentrum, University of Basel, Mattenstrasse 26, CH-4058, Basel, Switzerland
3: Laboratoire de Biologie Structurale de la Cellule, BIOC, UMR7654 CNRS/Ecole polytechnique, Palaiseau France
4: Plateforme de Bioinformatique, Université de Paris, FRC 550 CNRS, F-75005, Paris, France.
Institut de Biologie Physico-Chimique, F-75005, Paris, France.
5: Structural Bioinformatics Unit, Department of Structural Biology and Chemistry, C3BI, Institut Pasteur, CNRS UMR3528, CNRS USR3756, Paris, France.
6: Mass Spectrometry for Biology Unit, CNRS USR 2000, Institut Pasteur, 75015 Paris, France

Running title: Interaction specificity between ExbB and TonB/HasB

For correspondence: # Valérie Biou, valerie.biou@ibpc.fr,
Philippe Delepelaire, philippe.delepelaire@ibpc.fr

* Present addresses:
Véronique Yvette Ntsogo Enguéné: Department of Biochemistry, University of Cambridge, Tennis Court Road, Cambridge CB2 1GA, UK
Gisele Cardoso de Amorim: Instituto de Bioquímica Médica, Universidade Federal do Rio de Janeiro, Rio de Janeiro, RJ, Brasil.
Henning Stahlberg: Centre d'imagerie Dubochet UNIL-EPFL-UNIGE & Laboratoire de microscopie électronique biologique UNIL-EPFL, Lausanne, Switzerland

Abstract.

ExbB and ExbD are cytoplasmic membrane proteins that associate with TonB to convey the energy of the proton-motive force to outer membrane receptors in Gram-negative bacteria for iron uptake. The opportunistic pathogen *Serratia marcescens* (*Sm*) possesses both TonB and a heme-specific TonB paralog, HasB. $ExbB_{Sm}$ has a long periplasmic extension absent in other bacteria such as *E. coli (Ec)*. Long ExbB's are found in several genera of Alphaproteobacteria, most often in correlation with a *hasB* gene. We investigated specificity determinants of $ExbB_{Sm}$ and HasB. We determined the cryo-EM structures of $ExbB_{Sm}$ and of the ExbB-$ExbD_{Sm}$ complex from *S. marcescens*. $ExbB_{Sm}$ alone is a stable pentamer, and its complex includes two ExbD monomers. We showed that $ExbB_{Sm}$ extension interacts with HasB and is involved in heme acquisition and we identified key residues in the membrane domain of $ExbB_{Sm}$ and $ExbB_{Ec}$, essential for function and likely involved in the interaction with TonB/HasB. Our results shed light on the new class of inner membrane energy machinery formed by ExbB,ExbD and HasB.

52 **Introduction**

53

54 Transport of nutrients across the Gram-negative outer membrane is either a diffusion-facilitated
55 or an active process. In the latter case, the process is powered by the energy of the proton-
56 motive force (pmf) transmitted through the periplasm to specialized outer membrane (OM)
57 transporters (the so-called TBDT's, TonB dependent transporters). A complex of three
58 cytoplasmic membrane proteins, TonB, ExbB and ExbD, that together form the TonB complex
59 (see (1) for a review) conveys the energy of the pmf to the TBDT. In *Escherichia coli* K12,
60 there is only one set of *tonB, exbB* and *exbD* genes, whereas there are nine TBDT's (2), all
61 energized by the same complex. ExbB and ExbD respectively belong to the MotA-TolQ-ExbB
62 and MotB-TolR-ExbD protein families. Those proteins are involved in power generation and
63 transmission in various processes (MotAB drives flagellar rotation, the ExbB-ExbD complex
64 referred to as ExbBD energises active transport of molecules across OM receptors and TolQR
65 is involved in cell division), at the expense of pmf dissipation across the cytoplasmic membrane
66 (3-6). They form complexes that associate respectively with the flagellar rotor, TonB and TolA.
67 It has also been shown that ExbD does not accumulate in the absence of ExbB, and that TonB
68 does not accumulate in the absence of the ExbBD complex (7). The C-terminal domains of
69 TonB and ExbD reside in the periplasm and interact with each other (8, 9). ExbD TM (Trans-
70 Membrane segment) has one strictly conserved aspartate residue (10), which is thought to
71 undergo cycles of protonation/deprotonation (coupled to pmf dissipation) and is essential to its
72 function.
73 TBDT's comprise a 22-stranded ß-barrel anchored in the outer membrane. An N-terminal
74 domain folded inside the barrel, and called the plug, contains the main region of interaction
75 with TonB, the so-called TonB box, located in the N-terminal periplasm-exposed part of TBDT.

76 The N-terminus of TonB is localized in the cytoplasm, followed by a single transmembrane
77 segment, and by a Pro-Lys rich region long enough to span the periplasmic space and ends with
78 a structured C-terminal domain interacting with the TBDT TonB box. The substrate binds the
79 extracellular side of the TBDT receptor, triggering conformational changes that are transmitted
80 to the periplasmic side and allow the interaction between TonB and the TonB box of the TBDT,
81 leading to the substrate entry into the periplasm by a yet unknown mechanism. A rearrangement
82 of the plug domain has been proposed to occur creating a path for the substrate across the
83 TBDT.
84 In *Serratia marcescens*, a close relative of *E. coli*, in which about twenty potential TBDT's
85 were identified, there are at least two TonB homologs: an ortholog of $TonB_{Ec}$ (48% aminoacid
86 identity with $TonB_{Ec}$(11)) and HasB, a TonB paralog that is strictly dedicated to its cognate
87 outer membrane receptor HasR(12, 13). HasB has the same topology as TonB, and its C-
88 terminal domain interacts specifically with HasR with a circa (ca.) 40-fold higher affinity than
89 the corresponding TonB domain (14). The Has (heme acquisition system) system includes the
90 TBDT HasR, which recognizes both free heme and the high-affinity extracellular heme-binding
91 HasA hemophore. HasB is encoded within the *has* locus and displays low sequence identity
92 with either *E. coli* or *S. marcescens* TonB. The Has system has been functionally reconstituted
93 in *E. coli*. Unlike $TonB_{Sm}$, HasB could not complement $TonB_{Ec}$ functions (12), nor was it able
94 to drive heme entry *via* the HasR receptor in the presence of $ExbBD_{Ec}$. A gain of function
95 mutation in the TM domain of HasB was however isolated in *E. coli*, restoring heme entry *via*
96 HasR in the presence of $ExbBD_{Ec}$ (12). This mutation corresponds to a 6 base-pair duplication
97 leading to a longer TM segment for HasB by inserting AL into CLVLVLALHLLVAALLWP
98 resulting in CLVLVLALALHLLVAALLWP.

99 Recently several structures of *E. coli* ExbB and ExbBD have been solved, either by X-ray
100 crystallography or cryo-EM(14-16). All samples studied included ExbB and ExbD, but not all
101 showed an ordered structure of ExbD. In these structures, $ExbB_{Ec}$(14) appeared as a pentamer.
102 Each monomer of ExbB has three TM helices that extend into the cytoplasm, and with a highly
103 polarized charge distribution on the cytoplasmic side. The central pore is apolar, lined by TM
104 helices 2 and 3 of each monomer, creating a large hydrophobic cavity inside the structure.
105 Another study using X-ray crystallography, single-particle cryo-EM and electron diffraction on
106 two-dimensional crystals concluded that ExbB could undergo a pH-dependent pentamer to
107 hexamer transition, and that the hexameric ExbB could accommodate three ExbD TM segments
108 in its pore (15). A more recent cryo-EM study of ExbBD reconstituted in nanodiscs however
109 confirmed the $ExbB_5ExbD_2$ stoichiometry with two TM helices of ExbD identified in the ExbB
110 pore (16). This is consistent with previous DEER (Double Electron Electron Resonance) results
111 (15). Similarly, *Pseudomonas savastanoi* ExbBD exhibits the same stoichiometry (17).
112 Structures of the flagellar MotAB motor complexes (related to ExbBD) from several bacteria
113 (*Campylobacter jejuni, Bacillus subtilis, Clostridium sporogenes, Vibrio mimicus, Shewanella*
114 *oneidensis,* PomAB from *Vibrio alginolyticus*) were recently published. They all display a
115 $MotA_5MotB_2$ stoichiometry and share some topology elements with ExbBD complex (17, 18).
116 The discovery of HasB and its functional specificities prompted us to identify the ExbBD
117 complex that would function with it in *S. marcescens*. In this study, we identified the
118 orthologous $ExbBD_{Sm}$ and found that this complex is active with both HasB and TonB. We
119 characterised a new family of ExbB proteins with a long N-terminal extension whose presence
120 is strongly correlated to the presence of a *hasB* gene ortholog in the genome. We purified
121 $ExbB_{Sm}$ alone and $ExbBD_{Sm}$ and determined their structures by single-particle cryo-EM at 3.1
122 and 3.96Å resolution, respectively. We show that in both cases, $ExbB_{Sm}$ behaves as a stable

123 pentamer; in the $ExbBD_{Sm}$ complex, we observe two TM helices of $ExbD_{Sm}$ in the pore of ExbB
124 pentamer, as it was shown for the *E. coli* case. Using NMR measurements, we also show that
125 the N-terminal periplasmic extension specific to $ExbB_{Sm}$ interacts with the C-terminal globular
126 domain of HasB. Finally, *via* mutagenesis studies and bacterial growth assays, we show that
127 the first transmembrane helix TM1 of ExbB contains specificity determinants for interaction
128 with HasB/TonB and that the periplasmic extension of ExbB does play a role in heme
129 acquisition *via* the Has system.
130
131 **Results**
132 **1. Orthologs of *E. coli exbB* and *exbD* in *Serratia marcescens* define a new ExbB family**
133 **with an N-terminal extension.**
134 Sequence analysis of strain Db11, a fully sequenced *S. marcescens* isolate (GenBank: *Serratia*
135 *marcescens* subsp. marcescens Db11, complete genome. ACCESSION HG326223,
136 https://www.ncbi.nlm.nih.gov/nuccore/HG326223.1), identified one putative operon encoding
137 orthologs of *E. coli* ExbB and ExbD (SMDB11_3479(ExbD) and SMDB11_3480(ExbB)). In
138 *E. coli*, the *exbBD* operon is surrounded on the 5' side, and in the opposite direction, by *metC*
139 (encoding a cystathionine lyase) and on the 3' side by *yhgA* (encoding an aldehyde reductase).
140 In *S. marcescens* Db11, the *exbB*-like gene is close to and in the opposite orientation to a *metC*
141 homolog, as in *E. coli.* At the 3' end of the operon, and in the opposite direction there are genes
142 related to sucrose metabolism. Comparison of the coding sequences indicated that the *exbD*
143 gene encoded a 140 residue-long protein (71% identity with the 141 residue-long *E. coli*
144 sequence). In contrast, the putative *exbB* gene encodes a much longer protein than its *E. coli*
145 counterpart (325 residues instead of 244 residues in *E. coli*, 73% identity in the common part).
146 The additional stretch of residues present in $ExbB_{sm}$ is located at the N-terminus and

147 corresponds to a putative signal peptide followed by a ~50 residue N-terminal extension of the
148 mature protein (Figure 1A).
149 A BLAST search (19) on bacterial genomes indicated that such "extralong" ExbB's are found
150 in different Gammaproteobacteria, including *Serratia*, *Yersinia*, *Pseudomonas*,
151 *Erwinia*/*Dickeya*, and many genera in the Alphaproteobacteria class. Table I lists representative
152 species of Alphaproteobacteria in which such long ExbB's are found. Interestingly, about 90%
153 of the long ExbB-containing species listed in this table also have a *hasB* gene ortholog.
154 An alignment of these ExbB aminoacid sequences (represented as a Logo on Figure 1B) also
155 shows that the mature N-terminal extensions are of variable lengths between a few and 150
156 residues with an average of 50 residues. These extensions are quite rich in Ala (24,6%) and Pro
157 (14,5%) residues and therefore likely to be unstructured but could be involved in protein-protein
158 interactions as proline-rich regions often are in signalling processes (20-22).
159 The Conserved Domain Database (23) currently contains two ExbB subfamilies in the cI00568
160 MotA_ExbB superfamily, TIGR02797 (containing *E. coli* ExbB, as well as longer ExbB's) and
161 TIGR02805 (containing *Haemophilus influenzae* ExbB, with a very short cytoplasmic domain
162 between TM1 and TM2). Based on sequence data, TIGR02797 can be divided into 2 groups:
163 those with "extralong" ExbB's in one subfamily, and *E. coli*-like sequences in the other. Along
164 with the existence of HasB in the bacterial species, the identification of this N-terminal addition
165 prompted us to further characterise the ExbB-ExbD complex from *S. marcescens*.
166
167 **2. $ExbBD_{Sm}$ complements $ExbBD_{Ec}$ for iron acquisition and functionally associates with**
168 **both TonB and HasB for heme acquisition through HasR.**
169

170 As a first step in the characterization of the identified $ExbBD_{Sm}$, we tested whether this complex
171 complements $ExbBD_{Ec}$. To this end, the plasmids $pBADExbBD_{Sm}$ and $pBADExbBD_{Ec}$ were
172 constructed, introducing the two genes from *S. marcescens* or *E. coli*, into pBAD24 vector
173 under the control of arabinose-inducible P_{araBAD} promoter. By using growth under iron
174 starvation conditions as a test, we could show that $exbBD_{Sm}$ complements $exbBD_{Ec}$. The *E. coli*
175 C600Δ*exbBD* strain is indeed more sensitive than its wild-type counterpart to iron starvation
176 (induced for example by the Fe^{2+} chelator dipyridyl, DiP) as ExbBD are required to transduce
177 pmf to TonB for siderophore uptake. Its growth in the presence of DiP is restored by the
178 expression of either $pBADExbBD_{Ec}$ or $pBADExbBD_{Sm}$ (Figure 2).
179 We then tested the functionality of ExbBDSm in heme acquisition via the Has system
180 reconstituted in a heme auxotroph *E. coli* strain. To avoid interference from the chromosomal
181 *exbBD* operon and from *tonB*, we used the C600Δ*hemA*Δ*exbBD* and the
182 C600Δ*hemA*Δ*exbBD*Δ*tonB* strains, transformed with various recombinant plasmid pairs, one
183 bringing the complete Has locus, with or without the *hasB* gene, the other one with the *exbBD*
184 operon or its derivatives under the control of the P_{araBAD} promoter. In this kind of experiment,
185 the bacterial growth reflects both the expression of the various Has components under the
186 control of their own regulatory elements (24), and the efficiency of the heme uptake process
187 itself. Two kinds of tests were carried out, one on solid substrate in Petri dishes, allowing to see
188 haloes of bacterial growth around wells punched in the agar and containing the heme source,
189 the other one in liquid medium in microplates with an absorbance plate reader, allowing to
190 record growth at regular intervals over extended periods. The latter type of tests allows a more
191 precise and quantitative description of the phenotypes as it is realized in a homogeneous
192 medium, which is not the case with Petri dishes. Six strains were constructed: one set deleted
193 from TonB C600Δ*hemA*Δ*exbBD*Δ*tonB* (pAMHasISRADEB + pBAD24),

194 C600Δ*hemA*Δ*exbBD*Δ*tonB* (pAMHasISRADEB + pBADExbBD$_{Ec}$),
195 C600Δ*hemA*Δ*exbBD*Δ*tonB* (pAMHasISRADEB + pBADExbBD$_{Sm}$), and one set with TonB
196 C600Δ*hemA*Δ*exbBD* (pAMHasISRADE + pBAD24), C600Δ*hemA*Δ*exbBD* (pAMHasISRADE
197 + pBADExbBD$_{Ec}$), and C600Δ*hemA*Δ*exbBD* (pAMHasISRADE + pBADExbBD$_{Sm}$). The
198 ExbBD constructs for Ec and Sm are schematized on the first two lines of Figure 3A. The
199 results are reported in Figures 3B (Petri dishes, overnight observation), 3C (Petri dishes, 36h
200 observation) and 3D (microplates, recording over 66h). As expected, control strains (with
201 pBAD24) did not grow. ExbBD$_{Sm}$ was functional with both HasB and TonB (middle series of
202 holes in Figure 3C indicated with orange and blue dots, and orange and blue dots curves in
203 Figure 3D), although with quite dramatically different kinetics and yield, the onset of growth
204 occurring at 5-6hrs for the HasB-ExbBD$_{Sm}$ pair, and at 22-23hrs for the TonB-ExbBD$_{Sm}$ pair.
205 Moreover, the final OD of TonB-ExbBD$_{Sm}$ is half that of HasB-ExbBD$_{Sm}$. Under our
206 experimental setup, ExbBD$_{Ec}$ was also functional with both TonB and more surprisingly with
207 HasB (bottom series of holes in Figure 3C, and green and grey dots curves in Figure 3D), the
208 onset of growth occurred at around 15-16hrs for TonB, and 18hrs for HasB; however, the
209 maximal OD was lower for the HasB-ExbBD$_{Ec}$ pair (0.43 vs. 0.72). Finally, the ExbBD$_{Sm}$-
210 HasB pair seems less sensitive to iron starvation than all the other ones, since similar results
211 are obtained at 100 and 200µM Dipyridyl (Figure 3B), which is not the case for the other pairs,
212 as already observed in the TonB-ExbBD$_{Ec}$ case (25). These results might seem at odds with the
213 previous results obtained on HasB (12) which showed that HasB was nonfunctional with
214 ExbBD$_{Ec}$. However, the experimental setup was quite different, both in terms of plasmids used,
215 strains and conditions of observation. Therefore, ExbBD$_{Sm}$ is the *E. coli* ExbBD ortholog, able
216 to associate both with HasB and TonB$_{Ec}$.
217

218 **3. Characterization of $ExbB_{Sm}$ and $ExbBD_{Sm}$: Specific function of the N-terminal**
219 **extension of $ExbB_{Sm}$**

220 **3.a Purification and mass-spectrometry analyses of protein and associated lipids**

221 To gain further insight into the possible differences between $ExbBD_{Sm}$ and $ExbBD_{Ec}$, we
222 purified both $ExbB_{Sm}$ and $ExbBD_{Sm}$ (as C-terminal 6-His-tagged proteins on ExbB for ExbB
223 purification, and C-terminal 6-His tag on ExbD for ExbBD purification, see Materials and
224 Methods section) in LMNG (lauryl maltose neopentyl glycol) micelles (Figure 4, A and B).
225 Both $ExbB_{Sm}$ and $ExbBD_{Sm}$ appear as homogeneous oligomers at the last size exclusion
226 chromatography (SEC) step.

227 Mass spectrometry analysis showed that purified $ExbD_{Sm}$His6 has a mass of 16 131 Da close
228 to its theoretical mass of 16261.7 Da. Purified $ExbB_{Sm}$ has a measured mass of 29 557 Da and
229 its predicted mature sequence has a theoretical mass of 29556.8 Da. Together with the
230 determination of the first amino-acid residue for ExbB, this confirmed that the predicted signal
231 sequence of $ExbB_{Sm}$ is absent from the mature sequence and has therefore been processed. It
232 also showed that ExbD initial Met residue was cleaved off (see Supplementary Figure S1).
233 More interestingly, mass spectrometry analysis of chloroform/methanol extracts of the purified
234 proteins also showed that both complexes contained native lipids (Supplementary Figure S2),
235 mostly phosphatidylglycerol (PG) and phosphatidylethanolamine (PE), and that ExbBD also
236 contained some cardiolipin (CL) (Supplementary Figure S3). Further analysis of aliphatic chain
237 composition of lipids shows evidence of specific composition with a majority of PG with 34
238 carbons and 2 unsaturations (Supplementary Figure S4). Considering that the $ExbBD_{Sm}$
239 complex is functional in *E. coli*, and that the phospholipid composition of *S. marcescens* is quite
240 similar to that of *E. coli* (26), this affinity for lipids may disclose a specific recognition that
241 may be important for the function.

242 **3b NMR shows an interaction between $HasB_{CTD}$ and $ExbB_{Sm}$ periplasmic extension.**

243 The presence in $ExbB_{Sm}$ of an N-terminal extension residing in the periplasm led us to
244 investigate its function. This extension contains more than 50% of Ala and Pro residues and is
245 predicted to be unstructured by disorder prediction servers such as IUPRED2 (27). Indeed,
246 NMR analysis of a 44 residue-long synthetic peptide corresponding to this extension ($ExbB_{Sm}$
247 1-44) did not show any indication of secondary structure (our unpublished results). Since this
248 region is predicted to be in the periplasm where the C-terminal domain of HasB, $HasB_{CTD}$ is
249 also located, we investigated the potential interaction of the $ExbB_{Sm}$ 1-44 synthetic peptide with
250 $HasB_{CTD}$ by NMR. The analysis of chemical shift perturbations (CSP) of amide resonances of
251 $HasB_{CTD}$ upon addition of the peptide, showed that the chemical environment of their
252 corresponding residues was modified because of their interaction (Figure 5 A and
253 Supplementary Figure S5). Perturbed residues are mainly located on the helical face of $HasB_{CTD}$
254 forming a continuous surface of interaction (Figure 5B and 5C) (R175, R178-K180, K184,
255 Q192, T200, L201, Q204, H206, A232, A240, G246). Interestingly, this face is on the opposite
256 side of the third beta strand of HasB that was previously shown to interact with HasR (28). In
257 addition, the residues of a small pocket at the C-terminus of HasB (D255, R259) show also high
258 CSP and might be involved in the interaction with ExbB or subject to a conformation change
259 induced by this interaction.

260

261 **3c An $ExbB_{Sm}$ mutant devoid of the N-terminal extension is affected in its function.**

262 To assess the potential function of the N-terminal periplasmic extension of $ExbB_{Sm}$, we
263 engineered a $ExbB_{Smdelextss}$ mutant lacking this extension (Figure 3A) (see Materials and
264 Methods for details) and tested its effect on the growth of a C600Δ*hemA*Δ*exbBD*Δ*tonB* strain
265 harbouring plasmids pAMHasISRADEB and $pBADexbBD_{Sm}$ or its derivatives in liquid

266 culture. We observed that the lag between the start of the experiment and the onset of growth
267 is at least 2 hours longer for the $ExbB_{Smdelextss}$ mutant strain, as compared to the WT strain
268 (Figure 6A, compare orange and yellow curves) and a control strain (medium blue). In addition,
269 the maximum OD reached after growth is slightly but significantly decreased (Figure 6 A). To
270 ensure that this difference was not due to a difference of expression of the two constructs, we
271 compared their amounts in membrane preparations by immunodetection. As our anti-$ExbB_{Sm}$
272 antibody was not sensitive enough for this measurement, we used the His-tagged version of
273 $ExbB_{Sm}$ readily detectable with anti-His6 antibodies. Coomassie blue stained SDS-PAGE
274 showed that the 3 conditions have similar total amounts of protein (Figure 6B). The Western
275 blot shows that the amount of the $ExbB_{SmHis6}$ variant deleted of its N-terminal extension is at
276 least equal, if not slightly higher, to the amount of the wild-type protein (Figure 6C, lanes 2 and
277 3), ruling out a possible decrease in protein concentration. The N-terminal periplasmic
278 extension of $ExbB_{Sm}$, is therefore likely involved in the functioning of the Has system, whether
279 at the transcription activation of the Has locus, and/or at any later step.
280

281 **4 $ExbB_{Sm}$ and $ExbBD_{Sm}$ structural analysis by cryo-EM show $ExbB_5$ and $ExbB_5D_2$**
282 **stoichiometries.**

283 **4a $ExbB_{Sm}$ structure**

284 As $ExbB_{Sm}$ presented specific features compared to $ExbB_{Ec}$, we set out to determine its structure
285 by single-particle cryo-EM, see Material and Methods for details. The 3D class average model
286 clearly showed a pentameric structure. It was refined and polished to obtain a resolution of 3.1Å
287 using the Fourier shell correlation (FSC) gold-standard criterion at 0.143. Maps were refined
288 with and without C5 symmetry and showed a 98% correlation in density. Therefore, we chose
289 to use the map based on C5 symmetry for model building.

290 The structure solved here and shown in Figure 7 A (side view) and B (cytoplasm view), has the
291 same α-helix bundle topology and is very similar to that of *E. coli* ExbB 5SV0 structure (that
292 was co-purified with ExbD but did not show any ordered density for ExbD (14)), with a 1.3Å
293 root mean square deviation (rmsd) over all Cα atoms (Table II). This shows that $ExbB_{Sm}$ is
294 stable as a pentamer on its own. The periplasmic N-terminal extension did not yield any visible
295 density, precluding its structure determination. At the C-terminus of each monomer, however,
296 density was clearly defined, allowing structure determination for an additional 10 residues in a
297 helical conformation up to the last one (helix α8 finishing with Gly 283, see Figure 7C) before
298 the His-tag that is present but disordered. In the 5SV0 X-ray structure, a calcium ion, present
299 in the crystallisation solution, is bound to the five Glu 106 (of helix α2 in the TM region) on
300 the cytoplasmic side. In $ExbB_{Sm}$, this residue is replaced by an Asn, and we do not observe any
301 density that could be assigned to a metal ion.

302

303 The structure of the whole pentamer with one monomer coloured as a function of sequence
304 conservation in this sub-class of ExbB (Supplementary Figure S6) shows that the highest

305 residue conservation is inside the transmembrane channel, indicative of high functional
306 constraints, while the TM residues located at the membrane surface are more variable. The
307 same observation was made for ExbB sequences lacking N-terminal signal sequence and
308 periplasmic extension (14).
309 The cryo-EM density of $ExbB_{Sm}$ shows vents located at the interface of adjacent monomers and
310 at the height of the cytoplasmic junction with the inner membrane leaflet (Figure 7A). These
311 vents may allow solvent or ion passage. Additional density was also clearly observed on the
312 external surface, and we attributed it to the phospholipids present in the preparation. Each ExbB
313 monomer appears to be associated with the equivalent of two PG molecules, located at the inner
314 leaflet of the cytoplasmic membrane (Figure 7A, D and E). However, we were able to model
315 only one PG molecule per monomer with confidence. Three PE (phosphatidylethanolamine, the
316 major *E. coli* phospholipid) molecules and one PG molecule were identified as associated to
317 the ExbBD pentamer in the *E. coli* complex after reconstitution in nanodiscs (16). The cryoEM
318 density map, when displayed at a level that shows the detergent belt, shows density inside the
319 ExbB membrane pore (supplementary figure S7A). This density is too noisy to allow model
320 building (supplementary figure S7B). However, it corresponds to a region with positive
321 electrostatic charge on the top and bottom of the pore and neutral or hydrophobic in the middle
322 (supplementary figure S7C). This density could be due to the presence of lipid or detergent.
323 Interestingly, it is located at a different height as compared to the detergent belt and external
324 lipids. In summary, our cryo-EM structure shows that $ExbB_{Sm}$ is stable as a pentamer and
325 associates strongly with specific phospholipids coming from the inner leaflet of the membrane.
326 **4b $ExbBD_{Sm}$ structure**
327 We also solved the structure of the $ExbBD_{Sm}$ complex by cryo-EM (Figure 8 and Table II). As
328 for ExbB, the purified complex exhibited a symmetric peak on SEC (see Figure 4, B). Cryo-

329 EM data were collected and processed as described in the Material and Methods section. In
330 contrast to $ExbB_{Sm}$, 2D classes showed preferential orientations with 92% top views and only
331 8% side views. Due to this strong bias in particle orientation, the resolution achieved was 3.96
332 Å, precluding reliable positioning of the side chains. However, our $ExbB_{Sm}$ model fitted readily
333 into the density. As observed for $ExbB_{Sm}$ alone, in the $ExbBD_{Sm}$ complex, $ExbB_{Sm}$ behaves as
334 a pentamer, and no sign of other assemblies was found. Similarly, no density could be attributed
335 to the periplasmic extension. Two clear densities inside the $ExbB_{Sm}$ pore were assigned to the
336 pair of $ExbD_{Sm}$ TM segments (Figure 8 B and C). The charge distribution is highly polarised
337 on the cytoplasmic side: the region close to the membrane is positively charged and the distal
338 part is negatively charged as observed for $ExbB_{Ec}$ (Supplementary Figure S8A). The central
339 pore of $ExbB_{Sm}$ is apolar, lined by TM helices 2 and 3 of each monomer, creating a large
340 hydrophobic cavity inside the structure (Supplementary Figure S8B). The ExbD helices were
341 initially oriented similarly to $ExbD_{Ec}$ in structure 6TYI and remained stable during refinement.
342 Interestingly, the ExbD TM helices are at the same height as the density observed in the pore
343 of ExbB alone, and closer to the periplasm than the membrane bilayer. In the refined model,
344 Asp 25 from $ExbD_{Sm}$ monomer chain G faces Thr 218 from $ExbB_{Sm}$ chain C, while Asp 25
345 from the $ExbD_{Sm}$ chain F faces the interface between two $ExbB_{Sm}$ monomers A and E
346 (Supplementary Figure S8C and D). The estimation of pKa, by using the program Propka (29)
347 server, shows that Asp 25 has a pKa of 7.3 for chain F and 7.4 for chain G, both very peculiar
348 for solvent-accessible acidic residues but that can be found in buried active sites or membrane
349 proteins (30). This pKa should allow protonation and deprotonation of ExbD Asp 25 at
350 physiological pH.
351 As compared to the structure of $ExbB_{Sm}$, there is a slight «opening» towards the periplasmic
352 side (the distance of Ala 197 from one subunit to Leu 204 of the facing subunit varying from

353 25.5Å in $ExbB_{Sm}$ to 29.8Å in $ExbBD_{Sm}$, much greater than any error expected due to the
354 difference in resolution of the two structures). This opening of the structure is limited to the
355 periplasmic part (Supplementary Figure S9). The rmsd between $ExbB_{Sm}$ alone and in complex
356 with $ExbD_{Sm}$ is 2Å over all Cα of the pentamer, and the rmsd between $ExbB_{Sm}$ in complex with
357 $ExbD_{Sm}$ and $ExbB_{Ec}$ in complex with $ExbD_{Ec}$ (structure 6TYI chains A-E) is 1.7Å.
358 As compared to the 6TYI structure of *E. coli* ExbBD complex, we observe significant
359 differences that may be related to the specificity of function of $ExbB_{Sm}$. Both $ExbB_{Sm}$ and
360 $ExbBD_{Sm}$ inner pores are slightly wider than their *E. coli* counterparts at the periplasmic
361 entrance. Consequently, two channels cross the membrane region, (extending from the
362 periplasmic entrance to the Asp 25 residue from the ExbD TM deeply embedded in the ExbB
363 pore) that are clearly seen in the $ExbBD_{Sm}$ (as detected by the MoleOnline (31) Server, Figure
364 9, A and C; the average diameter is around 3Å) while the *E. coli* structure exhibits a single,
365 much thinner channel as detected with the same parameters of MoleOnline (Figure 9, B and D;
366 average diameter around 2Å). It is therefore possible that this structure represents another state
367 of the ExbBD motor complex, whereby the periplasmic side allows solvent access to the Asp
368 25 residue of ExbD TM. The different physico-chemical conditions (nanodiscs vs. detergent
369 micelles, 200 vs. 100mM NaCl, pH7,4 vs. pH8) might also influence such parameters.
370 In summary, we show that ExbBD from *S. marcescens* has a 5:2 stoichiometry with a larger
371 channel allowing solvent or proton transport from the periplasmic side as compared with the *E.*
372 *coli* structure.
373
374 **5. Swapping residues in TM1 between $ExbB_{Sm}$ and $ExbB_{Ec}$ strongly suggests that ExbB**
375 **TM1 interacts with HasB/TonB.**

376 As already mentioned, TBDT function requires a productive association between TonB or its
377 orthologs/paralogs with ExbBD complexes. It is known that the periplasmic domains of ExbD
378 and TonB interact, and there are both genetic and structural pieces of evidence for the
379 interaction between the TM helix of TonB and the first TM helix of ExbB. Our experimental
380 system gave us the opportunity to investigate the specificity determinants between HasB/TonB
381 and ExbB. Previous work (12) lends support to the absence of interaction between HasB and
382 $ExbBD_{Ec}$. However, our data rather favor a less efficient interaction between HasB and
383 $ExbBD_{Ec}$ than with $ExbBD_{Sm}$. *E. coli* can grow with the HasB-$ExbBD_{Ec}$ pair, although more
384 slowly and with a lower yield: the final OD was 0.78 for HasB-$ExbBD_{Sm}$ and 0.43 for HasB-
385 $ExbBD_{Ec}$ (Figure 3 D orange and grey curves). As it is known that ExbBD is required to
386 stabilize TonB, we first tested whether HasB was stabilized by ExbBD. We could show that,
387 although HasB does not accumulate in the absence of ExbBD, it is readily present in comparable
388 amounts with either $ExbBD_{Sm}$ or $ExbBD_{Ec}$ (Figure 10). This observation therefore indicates
389 that most likely HasB also interacts with $ExbBD_{Ec}$ so as to be stabilized (i. e., withstanding
390 proteolytic degradation), but in a less functional manner than with $ExbBD_{Sm}$.
391 A general framework put forward for the Mot complexes indicates that MotA (equivalent of
392 ExbB) rotation around MotB (equivalent of ExbD) drives the rotation of the flagellum basal
393 ring (17, 18). We tested the possibility that ExbB residues exposed at the surface of the protein
394 might be involved in a functional interaction with HasB/TonB, as has been proposed in the case
395 of the TonB-ExbBD complex from *P. savastanoi* (17). The superposition of residue
396 conservation on the structure of ExbB showed that the membrane-facing residues of the TM
397 region of helix α2 and the cytoplasmic residues were the least conserved (Figures 1 and S6).
398 We noted one conspicuous stretch of residues located in the cytoplasmic leaflet of TM helix 1
399 (see Supplementary Figure S6):

400 residues 76-88 of $ExbB_{Sm}$ TILFAKGSELLRA corresponding to

401 residues 39-51 of $ExbB_{Ec}$ AIFFSKSVEFFNQ

402 (identical residues are underlined) that is the least conserved one between the two proteins. In

403 this stretch, the conserved I, K and E residues point toward the innermost part of the protein

404 and the non-conserved residues point to the outside and are available for protein-protein

405 interaction (Figure 11 E and F).

406 We speculated that this region of ExbB might establish interaction with HasB. We made a

407 chimeric $ExbB_{Ec}$ protein, with its 39-51 region replaced by residues 76-88 from $ExbB_{Sm,}$ named

408 $ExbB_{Ec\text{-}Sm76\text{-}88}$, and asked how this chimeric $ExbB_{Ec}$ protein would allow growth in the presence

409 of HasB (see Figure 3A for the constructions), as compared to $ExbB_{Ec}$. As shown in Figure 6A,

410 this chimeric protein $ExbB_{Ec\text{-}Sm76\text{-}88}$ (green dots) was more active with HasB than $ExbB_{Ec}$ (grey),

411 the onset of growth took 14hrs compared to 18hrs for $ExbBD_{Ec}$ and the maximum OD was 0.74

412 compared to 0.43 for $ExbBD_{Ec}$. We also made the inverse change where the 76-88 region of

413 $ExbB_{Sm}$ was replaced by the 39-51 region from $ExbB_{Ec}$ ($ExbB_{Sm\text{-}Ec39\text{-}51}$, magenta). This mutant

414 has a degraded behaviour as compared to $ExbB_{Sm}$, since the onset of growth occurs at 19hrs

415 compared to 6hrs, and the final OD is 0.47, compared to 0.78. To better locate the region

416 responsible for specificity, we produced one additional mutant where only residues 76-84

417 (TILFAKGSE) from $ExbB_{Sm}$ were exchanged for residues 39-47 (AIFFSKSVE) from $ExbB_{Ec}$

418 yielding $ExbB_{Ec\text{-}Sm76\text{-}84}$ (see Figure 3 A). $ExbB_{Ec\text{-}Sm76\text{-}84}$ was quite comparable to $ExbB_{Ec\text{-}Sm76\text{-}88}$

419 (see deep-blue and green curves on Figure 6A). This 9-residue stretch is therefore sufficient to

420 alter $ExbB_{Ec}$ to be better adapted to HasB. This set of experiments shows that the

421 intramembrane functional zones of ExbB are crucial for the growth of *E. coli* in our

422 experimental set up and therefore likely govern the interaction between ExbB and HasB.

423 In summary, we showed using NMR and culture growth assays that $ExbB_{Sm}$ N-terminal
424 extension (section 3b) and a few residues in the α2 helix TM region (section 5) are likely
425 involved in specific interactions with HasB.
426
427 **Discussion**
428 1) $ExbBD_{Sm}$ is a 5:2 complex at pH 8.
429 Our structures were solved at pH 8, and examination of the 2D class averages only showed
430 pentameric structures and not hexameric ones, contrarily to what has been observed in the
431 Maki-Yonekura study, where ExbB was mostly seen as a hexamer in the high pH regime (15).
432 In their study, the solubilizing detergent was DDM, that was subsequently exchanged for either
433 C8E4 or C10E5. These shorter chain detergents might have led to some destabilization of the
434 pentameric structure and provoked the conversion to the hexameric form. Our data agree with
435 those published by Lloubes, Buchanan et al. (14, 16). *In vivo*, a stoichiometry of 7ExbB, 2ExbD
436 and 1TonB has been determined in *E. coli* (32). Although one cannot completely rule out some
437 bias in this indirect measurement, a physiologically relevant reason for an excess of ExbB
438 would be to provide a permanent scaffold to which TonB and/or ExbD could associate with,
439 upon TonB complex dissociation, that might occur during the catalytic cycle, as has already
440 been proposed (33).
441 2) ExbB and ExbBD are co-purified with endogenous lipids.
442 In their last study, Celia *et al.* reconstituted ExbBD from *E. coli* into nanodiscs with added
443 phospholipids from *E. coli*, and found mostly PE bound to ExbBD (16). It is unclear whether
444 this phospholipid was a genuine tightly bound, co-purified lipid or whether it came from the
445 lipids added during reconstitution in the nanodiscs. In our case, we did not add any lipid and
446 our mass spectrometry identification of co-purified lipids found mostly PG and some PE in the

447 ExbB case (and CL for ExbBD). The cryo-EM structure shows that they are located in the inner
448 leaflet, as in the *E. coli* complex. PG and CL are negatively charged, whereas PE is zwitterionic.
449 This might be pertaining to the functioning of the complex, as the lipids are bound to a highly
450 positively charged interface, very close to the fenestrations seen in the structure and PE might
451 therefore be less tightly bound than PG or CL. Further analysis by mass spectrometry of the
452 aliphatic chains of the lipids present in our sample also revealed a specific composition in their
453 length and unsaturated nature.
454 One point also worth mentioning is the existence of "channels" inside the ExbBD tunnel,
455 potentially allowing the passage of proton/hydronium ion up to the Asp 25 residue of ExbD,
456 deeply embedded in the apolar medium of ExbB, and therefore with a pKa close to
457 physiological pH, allowing easy protonation/deprotonation steps of Asp 25 side chain. The
458 identified channels connect the cytoplasm to the periplasm *via* Asp 25, allowing us to propose
459 a possible trajectory for the proton transfer via those channels.
460 3) Motor model proposal
461 Regarding the coupling of the pmf dissipation with the mechanical work carried out by
462 MotAB/TolQR/ExbBD complexes, several models have been put forward that might be more
463 or less easy to reconcile with the structural data. A detailed mechanism was proposed for *C.*
464 *jejuni* MotAB complex, where cycles of protonation/deprotonation of the conserved Asp of the
465 MotB TM (equivalent to the conserved Asp 25 of the ExbD TM) are coupled to the rotation in
466 discrete steps of the MotA pentamer around MotB axis, provided that the periplasmic domain
467 of MotB is anchored to the peptidoglycan layer *via* its peptidoglycan binding site (18). Our
468 ExbBD structure indeed shows that ExbD monomers have two orientations relative to ExbB:
469 Asp 25 from one monomer faces Thr 208 of ExbB and Asp 25 from the second monomer faces
470 a hydrophobic region at the interface of two ExbB monomers. In the first state previously

471 protonated Asp25 could be deprotonated in contact with polar Thr208 while the second,
472 deprotonated Asp 25, could pick a proton from the periplasm via the channel. Rotation of the
473 the ExbB pentamer around the two ExbD chains would then lead to a new
474 protonation/deprotonation cycles accompanied by a change in the environment upon rotation.
475 How is this rotative energy conveyed to the TBDT?
476 The binding of an iron-loaded substrate on the extracellular binding site of a TBDT triggers a
477 reaction cascade ultimately leading to the substrate entry into the periplasm. The inner
478 membrane TonB(HasB) complex conveys the energy of the pmf to the TBDT most likely by a
479 rearrangement of the plug inside the barrel to allow substrate access to the periplasm and its
480 capture by periplasmic binding proteins. Specific interactions between the TonB(HasB) box of
481 the receptor and the C-terminal domain of TonB(HasB) are essential in this process (28). A
482 wealth of data has also accumulated documenting specific interactions between $TonB_{CTD}$ and
483 $ExbD_{CTD}$, depending upon the energy state of the cell. It is also known that ExbD and TonB
484 interact *via* their periplasmic parts (34) and in particular residue 150 of TonB (positioned just
485 upstream the C-terminal globular domain) can make cross-links to the C-terminal domain of
486 ExbD (35). There have also been indications and suggestions that both $TonB_{CTD}$ and $ExbD_{CTD}$
487 could interact with the peptidoglycan sacculus, providing anchor points to allow force
488 transmission. Molecular modelling works hypothesized that the C-terminal domain of TonB
489 (36) and the C-terminal domain of ExbD (37) have specific binding sites for the peptidoglycan
490 network. Atomic force microscopy experiments also showed that by exerting a pulling force on
491 the C-terminal domain of TonB bound to the BtuB TBDT, a partial unfolding of the TBDT plug
492 occurs, potentially leading to the entry of the substrate in the periplasm (38). Our NMR results
493 also show that ExbB interacts *via* its alanine and proline-rich periplasmic N-terminal region
494 with the HasB periplasmic domain on the side opposite to that of the TonB box interaction, thus

495 rendering a tripartite interaction possible. Our *in vivo* growth results with the $ExbB_{Smdelextss}$
496 mutant devoid of the periplasmic extension point to a possible role of the N-terminal
497 periplasmic extension in the activation of the transcription of the Has locus (figure 6).
498 The MotA-MotB model also posits that MotA outer region interacts with the rotor of the
499 flagellum and thus that MotA rotation drives the rotation of the flagellum. Similarly, the MotAB
500 rotating model can be extrapolated to the ExbBD complex. In this model, ExbB would rotate
501 around ExbD, driving the rotation of TonB/HasB thanks to the specific interaction between
502 TonB/HasB TM and ExbB TM α2. This kind of interaction is supported by our mutagenesis
503 data, as we could strongly increase the efficiency of $ExbB_{Ec}$ with HasB by exchanging a short
504 stretch of residues between $ExbB_{Sm}$ and $ExbB_{Ec}$. It is also in line with a previous TonB TM
505 point mutant partially suppressed by an ExbB α2 point mutant (39). Structure comparison of
506 the swapped regions shows that $ExbB_{Sm}$ has smaller residues that may be better accommodated
507 and less specific than the *E. coli* sequence (Figure 11, compare structures on figures 11C and
508 11D and helical wheels on figures 11E and 11F). Similar interactions have been proposed by
509 Deme et al. on the TonBExbBD complex from *P. savastanoi* (17), where an extra cryo-EM
510 density is seen outside the ExbB pentamer and was tentatively assigned to the TM domain of
511 TonB. The residues from $ExbB_{Ec}$TM1 (S34 and A39) identified as co-evolving with TonB TM
512 region (18) are only a little deeper in the bilayer than the residues we exchanged between
513 $ExbB_{Ec}$TM1 (39-51) and $ExbB_{Sm}$TM1, that are closer to the cytoplasm. More specifically,
514 whereas S34 is conserved between $ExbB_{Ec}$ and $ExbB_{Sm}$ (S71), A39 is replaced by T76.
515 Moreover, the hydrophobic core of HasB TM is likely shorter than that of TonB as seen in the
516 sequence alignment of HasB and TonB TM domains:
517

```
518  HasBSmTM 18-39 RRC---LVLVLALH-LLVAALLWPRR
519  TonBSmTM 10-34 RRISVPFVLSVGLHSALVAGLLYAS-
520  TonBEcTM  7-31 RRFPWPTLLSVCIHGAVVAGLLYTS-
521  consensus      RR      L   LH   VA LL
522
```

523 This difference in length might influence the orientation of HasBTM inside the bilayer and
524 potentially explain the gain of function of HasB6 mutant (in which the hydrophobic core has
525 two more residues (39)) to be better suited to $ExbB_{Ec}$ than HasB. The presence of a proline
526 residue in the TonB TM may also change its shape and the interaction with ExbB.
527 Several models have been proposed to account for the functioning of the TonB complex, in
528 conjunction with the entry of a substrate bound to the extracellular side of a given receptor. In
529 a first model, piston-like movements of TonB drive the unfolding of the plug inside the receptor
530 barrel. *In vivo* proteolysis studies indicated that the C-terminal domain of TonB can change
531 conformations during the catalytic cycle of protonation and deprotonation of the conserved Asp
532 residue in ExbD TM (40). In addition, the periplasmic linker between the TM helix and the C-
533 terminal domain of TonB is rich in Pro and Lys residues and might adopt an extended
534 conformation of a sufficient length to span the periplasm (41). We therefore propose a model
535 in which the force generated through the rotation of HasB/TonB, driven by ExbB rotation
536 around ExbD, is not directly transmitted to the TonB box of the receptor, but could be mediated
537 by the C-terminal domain of ExbD, that might act as an anchor point allowing force
538 transmission and converting the rotation into a pulling force exerted on the TonB/HasB box of
539 the receptor. Further studies are needed to test this model, in particular concerning protein-
540 peptidoglycan interactions, the force needed to trigger TBDT plug opening, and how to
541 distinguish between a rotation and a piston movement. Finally, given the wide range of lag
542 periods we observe in our growth curves using different combinations of ExbB TM1 mutants

543 and TonB/HasB, one may hypothesize that the membrane interaction between ExbB and
544 TonB/HasB influences the rate of transcription activation of the Has locus.
545 It is likely that the *in vivo* entry of a siderophore is a rather slow process: during a cell division
546 time a bacterial cell must take up ca. 300000 iron atoms from its surroundings. Under full
547 induction, there are roughly 10-15000 FepA siderophore receptors per cell and 1500 TonB
548 complexes (32), meaning that each receptor has to undergoes 20 cycles during a generation
549 estimated to 30 minutes, leading to a turnover time of the TonB complex of about 5-10 seconds.
550 As compared to flagellar motor that can operate at extremely high speeds (several hundred of
551 rotations per second), even though the basic mechanisms are likely to be conserved with the
552 ExbBD/TonB-HasB complex, it is much slower, which likely points to different coupling
553 mechanisms.
554
555
556 **Material and Methods**
557
558 **Strains and plasmid construction**
559 Strains, plasmids, and oligonucleotides used are shown Table III.
560 -Plasmid pBADExbBD$_{Sm}$ was constructed after amplification on the genomic DNA from strain
561 *S. marcescens* Db11 of a ca. 1.42kb fragment using primers ExbBDSm5' and ExbBDSm3'.
562 The PCR product was purified digested with *Eco*RI and *Sph*I, and ligated with pBAD24
563 digested with *Eco*RI and *Sph*I. Correct clones were selected after sequencing of the insert.
564 -Plasmid pBADExbBD$_{Sm}$His6 (encoding ExbB$_{Sm}$ and a C-terminally His-tagged version of
565 ExbD$_{Sm}$) was constructed by first amplifying on pBADExbBDSm a ca. 0.4kb fragment with
566 the following oligonucleotides SphIHisCtexbDSm and BglIIexbDSm; after amplification, the
567 fragment was purified, digested with *Bgl*II and *Sph*I, and ligated with pBADExbBDSm digested

568 with the same enzymes. The correct clones were selected after sequencing of the insert. In
569 biological tests, this plasmid was undistinguishable from its parent plasmid pBADExbBDSm.
570 -Plasmid pBADExbBD$_{Ec}$ was constructed by amplification on genomic MG1655 DNA of a ca.
571 1.7kb fragment with the following oligonucleotides ExbBD5c, and ExbBD3c; the PCR product
572 was purified, digested with *Eco*RI and *Sph*I, and ligated with pBAD24 digested with the same
573 enzymes. Correct clones were selected after sequencing.
574 -Plasmid pBADExbB$_{Sm}$His6 (encoding a C-terminally His-tagged version of ExbB$_{Sm}$) was
575 constructed as follows: a PCR fragment was amplified on pBADExbBDSm with the oligos
576 PBADFOR and ExbBHis6, digested with *Eco*RI and *Sph*I, and ligated with pBAD24 digested
577 with the same enzymes. Correct clones were selected by sequencing.
578 Plasmid pBADExbBD$_{Ec\text{-}Sm76\text{-}88}$ (encoding a chimeric ExbB$_{Ec}$ protein with its 39-51 residues
579 exchanged for the 76-88 residues from ExbB$_{Sm}$ and ExbD$_{Ec}$) was constructed as follows:
580 Plasmid pBADExbBD$_{Ec}$ was amplified with the two following 5' phosphorylated
581 oligonucleotides: ExbBEcSm76-88.1 and ExbBEcSm76-88.2. After digestion with *Dpn*I and
582 self-ligation, correct clones were selected by sequencing and the mutated fragments recloned
583 in pBAD24.
584 Plasmid pBADExbBD$_{Ec\text{-}Sm76\text{-}84}$ (encoding a chimeric ExbB$_{Ec}$ protein with its 39-47 residues
585 exchanged for the 76-84 residues from ExbB$_{Sm}$ and ExbD$_{Ec}$) was constructed in the same
586 manner, with the following oligonucleotides pairs: ExbBEcSm 76-84.1 and ExbBEcSm 76-
587 84.2.
588 In the same manner, plasmid pBADExbBD$_{Sm\text{-}Ec39\text{-}51}$ (encoding a chimeric ExbB$_{Sm}$ protein with
589 its 76-88 residues exchanged for the residues 39-51 from ExbB$_{Ec}$ and ExbD$_{Sm}$) was constructed
590 by PCR on the pBADExbBD$_{Sm}$ plasmid with the following couple of 5' phosphorylated
591 oligonucleotides: ExbBSmEc39-51.1 and ExbBSmEc39-51.2.

592 Plasmid pBADExbBD$_{Smdelextss}$ (encoding ExbB$_{Sm}$ deleted of its periplasmic extension and
593 ExbD$_{Sm}$) was constructed similarly, by using as a template pBADExbBDSm, with the two
594 phosphorylated oligonucleotides ExbBdelextss1 and ExbBdelextss2.
595 To construct pBADExbB$_{Smdelextss}$His6, a ca. 0.6kb *Eco*RI-*Kpn*I fragment from
596 pBADExbBD$_{Smdelextss}$ was exchanged for the corresponding fragment of pBADExbBHis6.
597 Plasmid pAMHasISRADEB (encoding HasI, HasS, HasR, HasA, HasD, HasE and HasB), was
598 constructed by digesting pAMHasISRADE (encoding HasI, HasS, HasR, HasA, HasD and
599 HasE) and pSYC7 (encoding HasD, HasE and HasB) (42) by *Kpn*I and *Hin*dIII, and purifying
600 fragments of respectively ca. 9 and 7 kbases, ligating them together to obtain a plasmid with
601 the whole *has* locus on a low copy number plasmid (pAM238) under the control of its
602 endogenous regulation signals (a fur box upstream of *hasI* and *hasR*, the *hasI* and *hasS* genes
603 respectively encoding the has specific sigma and anti-sigma factors, and the hasS box upstream
604 of *hasS* and *hasR*).
605 All constructions were carried out in *E. coli* strain XL1-Blue.
606 Strains and other plasmids used in this study are shown in Table III and are from the laboratory
607 collection.
608
609 **Protein expression and purification**
610 The BL21DE3(pExbBD$_{Sm}$His6/pBAD24) or BL21DE3(pExbB$_{Sm}$His6/pBAD24) were grown
611 at 37°C either in TB or MDM medium, and induced with 0.2% arabinose at 1.5-2OD600nm
612 (TB) or 5-6OD600nm (MDM) and the incubation continued for 3hrs. The cells were harvested
613 by centrifugation (10000g 20minutes 4°C), washed once in 20mMTris-HCl pH8.0, flash-frozen
614 in liquid N_2 and kept at -80°C. Cells were broken in a Cell disruptor (Constant, UK) at 1kbar
615 (10g of cells in 40ml final of 20mM Tris pH 8.0 containing protease inhibitor (Roche, EDTA

616 free), at 4°C. Benzonase was added and after ca. 15 minutes, the solution was centrifuged for
617 1hr at 100000g at 4°C. The pellet (crude membrane preparation) was resuspended in 20mM
618 Tris pH 8.0 plus protease inhibitor cocktail (Roche EDTA free), flash-frozen in liquid N_2 and
619 kept at -80°C.
620 The crude membrane preparation was solubilized in 20mM Tris pH 8.0, 20mM Imidazole,
621 100mM NaCl, 10% Glycerol, 0.8% LMNG (10g of equivalent whole-cell pellet solubilized in
622 40ml), plus protease inhibitor cocktail (Roche EDTA-free) for 30 minutes at 15°C. After
623 centrifugation (1hr 100000xg), the supernatant was incubated with 2.5ml Ni-Agarose beads
624 (Thermo-Fisher His-Pure Ni-NTA #88222) preequilibrated with the same buffer except for the
625 detergent concentration (0.0015% LMNG). After three hours of incubation on a rotating wheel
626 at 4°C, the beads were washed three times with 25ml of pre-equilibration buffer and then eluted
627 with two times 25ml of the pre-equilibration buffer containing 200mM Imidazole. The eluate
628 was concentrated and washed on 100kDa cut-off centrifugal device, in pre-equilibration buffer
629 without NaCl and Imidazole. The resulting sample was loaded on a monoQ HR10-100 column
630 equilibrated with 20mM Tris pH 8.0, 10% glycerol, 0.0015%LMNG and eluted with a gradient
631 from 0 to 1M NaCl in the same buffer. Peak fractions were collected and concentrated as before.
632 The concentrated sample was then loaded on a Superose 6 increase column equilibrated with
633 20mM Tris pH8.0, 100mM NaCl, 0.0015%LMNG. The peaks fractions were collected,
634 concentrated and their concentration determined by using the theoretical absorption coefficient
635 of either ExbB5D2 (113790$M^{-1}cm^{-1}$), or ExbB5 (104850$M^{-1}cm^{-1}$). They were then kept frozen
636 at -80°C in aliquots until use. The SEC profiles as well as a gel of a representative sample after
637 purification are shown in Figure 4. Previous attempts with DDM instead of LMNG yielded
638 similar results, and LMNG was chosen, owing to its very low CMC and its lower background
639 in cryo-EM.

640

641 **Activity tests**

642 Three types of tests were used, either in liquid medium or on agar plates.

643 1. Growth tests in liquid medium: *E. coli* C600 and its Δ*exbBD* derivatives were transformed
644 with specified plasmids and their growth tested in liquid LB medium at 37°C, at various
645 dipyridyl concentrations to induce iron starvation. OD_{600nm} was measured after overnight
646 growth.

647 2. Growth tests on plates: the relevant plasmids were also transformed into *E. coli* C600 Δ*hemA*,
648 a heme auxotroph strain (and derivatives thereof), and growth of the strains was assayed as
649 follows. Briefly, cells were first grown in LB medium (supplemented with delta-aminolevulinic
650 acid (50µg/ml) to bypass the effect of the Δ*hemA* mutation) at 37°C up to an OD_{600nm} of 1, and
651 then mixed with melted top agar (0.6%agar in LB), and poured onto LB agar plates containing
652 the appropriate antibiotics with arabinose at a concentration of 40µg/ml to induce expression
653 of the genes under the P_{araBAD} promoter(43). Wells, punched with Pasteur pipettes were filled
654 with heme-albumin (at 5, 1 or 0.2µM), at two dipyridyl concentrations (100 or 200µM) to
655 induce iron starvation. Plates were incubated overnight at 37°C and scored for growth around
656 the wells. All experiments were performed in triplicate.

657 3.Growth curves in liquid medium: a few colonies of *E. coli* C600
658 Δ*hemA*Δ*tonB*Δ*exbBD*(pAMHasISRADEB + pBAD24 or derivatives thereof) were first
659 inoculated in 4ml of LB medium at 37°C with the corresponding antibiotics, and 100µM
660 dipyridyl, 4µg/ml arabinose but without delta-aminolevulinic acid. Once the culture reached an
661 OD_{600nm} of ca. 1.2-1.5, it was diluted and inoculated in 48 well Greiner plates, in the same
662 medium to which was added 0.4µM He-BSA, as a heme source. The initial OD_{600nm} of the
663 cultures was 0.001. Each well contained 300µl of growth medium. Duplicates of each strain

664 were made, and the plate was incubated at 37°C with vigorous shaking (500rpm) in a Clariostar
665 Plus Microplate reader. OD_{600nm} was recorded every 30 minutes for 60-70 hours.
666

667 **N-terminal sequencing**

668 The N-terminus of $ExbB_{Sm}$ was determined at the Plateforme Protéomique de l'institut de
669 microbiologie de la Méditerranée (Marseille), after blotting on a PVDF membrane of a purified
670 sample of $ExbBD_{His6}$ run on SDS-PAGE and determined to be APAAN.

671 **Lipid extraction**

672 Chloroform (0.20 mL) and methanol (0.40 mL) were sequentially added to a sample of the
673 ExbB or ExbBD complex (0.1 mL). The sample was vortexed for 10 min at room temperature
674 and chloroform (0.2 mL) and water (0.2 mL) were further added. The organic phase was
675 collected and the extraction procedure was repeated on the remaining aqueous phase. Combined
676 organic layers were evaporated to dryness under argon and stored at -20 °C.

677 **Mass Spectrometry**

678 Dry lipid extracts obtained from ExbB, the ExbBD complex or from an *E. coli* lysate were
679 solubilized in chloroform/methanol (50/50). Samples were then nano-electrosprayed using a
680 TriVersa NanoMate (Advion Biosciences, Ithaca, USA) coupled to a Synapt G2-Si mass
681 spectrometer (Waters Corporation, Manchester, UK). The instrument was calibrated in negative
682 ion mode (for lipids) and positive ion mode (for proteins) from 50 m/z to 2000 m/z with NaI
683 (50 mg/ml) with an accuracy of 0.8 ppm in resolution mode. The following settings were
684 chosen: sampling cone 40 V, source offset 40 V, source temperature 80°C, trap gas flow 5
685 mL/min, helium cell gas flow 180 mL/min. MS/MS spectra were recorded using CID (Collision

686 Induced Dissociation) with a normalized collision energy set up to 30. To measure the mass of
687 the intact proteins of the ExbBD and purified ExbB complexes, a desalting step was performed
688 using micro Bio-Spin™ 6 (BIO-RAD) with 500mM ammonium acetate. Both samples were
689 analyzed in denaturing conditions after a two-fold dilution with acetonitrile 4% formic acid.
690 Mass spectra were acquired in positive ion mode. All molecular weights were measured after
691 MaxEnt1 software deconvolution into neutral species.

692 **Cryo-EM grid preparation and data acquisition**

693 3 µL of either purified $ExbB_{Sm}$ or $ExbBD_{Sm}$ complex at ca. 1 mg/mL was applied to C-Flat
694 1.2/1.3 holey carbon grids (Protochips Inc., USA) previously glow-discharged in air for 30s.
695 Grids were blotted for 2s at blot force 1 and vitrified in liquid ethane using a Vitrobot mark IV
696 (FEI company) operated at 10 °C and 100% relative humidity.
697 All data collection was performed with a Titan Krios (ThermoFisher Scientific) operated at 300
698 kV equipped with a K2 Summit direct electron detector (ThermoFisher Scientific) at the
699 European synchrotron research facility, ESRF (Grenoble, France). Movies were recorded in
700 electron counting mode with EPU software (ThermoFisher Scientific), aligned with
701 MotionCorr2 (44) and aligned images were processed with Gctf (45) using Scipion
702 interface(46).
703 For ExbB data collection, 4567 movies were collected at a magnification of 165000x with a
704 nominal pixel size of 0.827Å using a defocus range from -1.5 to -2.5µm. Movies of 56 frames
705 were acquired using a dose rate of 8 electrons/$Å^2$/second over 7 seconds, yielding a cumulative
706 exposure of 55.95 electrons/$Å^2$.

707 For ExbBD data collection, 4043 movies were collected at a nominal magnification of 139000
708 x with a pixel size of 1.067Å. Movies of 48 frames were acquired using a dose rate of 4.6
709 electrons/$Å^2$/second over 12 seconds yielding a cumulative exposure of 55.2 electrons/$Å^2$.
710
711 **Cryo-EM image processing and analysis**
712 **a) ExbB**
713 For ExbB, aligned movies were processed with Gctf (45) and only images with a resolution
714 higher than 4Å were kept; after visual inspection of the remaining images, processing was
715 carried out with Relion-3 (47) (Supplementary Figure S10). Particles were extracted using a 2-
716 fold binning, issued from a manual picking and a 2-D classification of particles picked out from
717 50 images. Automatic extraction was performed using the selected 2D class averages. After
718 several rounds of 2D and 3D classification, 161k particles were selected for 3D refinement.
719 They were corrected for local motion using Bayesian polishing option in Relion-3 and a post-
720 refined map produced a 3.1Å overall resolution with a 5-fold symmetry.
721 A homology model was built with the *Serratia marcescens* ExbB sequence using Phyre2 server
722 from 5SV0 monomer and docked into the refined map. Refinement was done with Phenix Real
723 Space Refine option with secondary structure, "non-crystallographic symmetry" and
724 Ramachandran restraints (48) and graphically adjusted with Coot (49). Lipid phosphatidyl
725 glycerol starting structure and geometry were built using Phenix eLBOW (50) and was fit in
726 the map using Coot then refined along with the protein model in Phenix.real_space_refine.
727
728 **b) ExbBD**
729 The data processing is summarised in Supplementary Figure S11. Movies were drift-corrected
730 and dose-weighted using MotionCorr2 (44). Aligned dose weighted averages were imported

731 into Cryosparc2 (51) and contrast transfer function was estimated using CTFFIND4.1 (52).
732 Micrographs with poor CTF estimation statistics or high drift profiles were discarded. The
733 remaining 3028 micrographs were used for automated particle picking. Particles were extracted,
734 Fourier cropped to 2 Å/px and 2D classified. The best 2D classes were used as templates for
735 automated particle picking resulting in 1.3 million particles. After several rounds of
736 classification, the best 600k particles were submitted to 3D classification by means of multi-
737 class ab-initio Reconstruction and Heterogeneous Refinement. 158 k particles belonging to the
738 best resolved classes were corrected for local motion, re-extracted and used in Non-Uniform
739 Refinement. The resulting refined map has a nominal resolution of 4.56 Å.
740 Based on the previous map a soft mask lining the micelle was designed in UCSF Chimera (53)
741 and used to signal subtract the corresponding micelle density of particles in the refined map.
742 Localized refinement of the signal subtracted particles produced a map of the complex with an
743 estimated resolution of 3.96 Å judging by FSC at 0.143 criterion. Data have been deposited
744 both at the EMDB and PDB databases (EMDB 10789 and 11806, PDB 6YE4 and 7AJQ, for
745 $ExbB_{Sm}$ and $ExbBD_{Sm}$ respectively, see Table II for refinement statistics).
746 Unless otherwise specified, the structure figures were made using UCSF Chimera software
747 (53).
748
749 **NMR experiments**
750 The C-terminal periplasmic domain of HasB, $HasB_{CTD}$ comprising residues 133-263, was
751 produced and purified as previously reported (28, 54). The peptide corresponding to the
752 periplasmic extension of $ExbB_{sm}$
753 (A_1PAANPAVTESVAPTTAPAPAAAAPESITPVNPAPTIQPPETRG$_{44}$- numbering with
754 reference to the mature protein) was synthetized by *Proteogenix*.

755 NMR experiments were acquired at 293 K on a 600 MHz Bruker Avance III spectrometer
756 equipped with a TCI cryoprobe. The spectra were processed with NMRpipe (55) and analyzed
757 with CcpNmr Analysis 2.4 software (56). Proton chemical shifts were referenced to 2,2-
758 dimethyl-2-silapentane-5 sulfonate as 0 ppm. ^{15}N were referenced indirectly to DSS (57)
759 (Wishart et al., 1995). $^{1}H–^{15}N$ HSQC experiments were acquired on 0.15 mM $HasB_{CTD}$ in
760 50mM sodium phosphate pH 7, 50 mM NaCl with or without the peptide. Aliquots from a
761 solution of peptide at 25mg/ml in the same buffer were added to the protein sample at 2:1 and
762 10:1 ratios. Chemical shift perturbations (CSPs) of backbone amide cross-peaks were
763 quantified by using the equation $CSP = [\Delta \delta H^2 + (\Delta \delta N \times 0.15)^2]^{1/2}$, where $\Delta \delta H$ and $\Delta \delta N$ are
764 the observed ^{1}H and ^{15}N chemical shift differences between the two experimental conditions.
765 The ^{1}H and ^{15}N resonance assignments were from Lefevre et al 2007 (58).
766
767 **Other biochemical methods**
768 SDS-PAGE and immunodetection with anti-HasB or anti-His6 antibodies (Abcam [HIS.H8]
769 (ab18184)) on whole cells or membrane preparations were carried out following standard
770 protocols. Secondary antibodies were coupled to alkaline phosphatase.
771
772 **BLAST search**
773 $ExbB_{Sm}$ was used as a search for BLAST for orthologs in complete bacterial genomes, focusing
774 on "long" ExbB's. Top hits were in *Serratia*, *Yersinia*, *Dickeya*, *Erwinia* and *Pseudomonas*.
775 Those genera were later excluded from successive BLAST searches to obtain orthologs in other
776 genera with higher p-value.
777
778 **Author contribution**

PD and VB conceived the study and wrote the manuscript. all authors contributed to the manuscript and approved it. PD produced protein samples and performed microbiology experiments. MC performed electron microscopy sample screening and data collection. RJDA, PDC, VYNE and VB processed cryo-EM data. VB built structural models. VB and PD interpreted models. BL installed and tested programs. CM and JCR performed mass spec analyses. NIP and GCA performed NMR analyses. HS provided advice with data collection and processing.

Data availability

Protein structures were deposited to the protein data bank with ID 6YE4 and 7AJQ. Electron microscopy maps were deposited to the EMDB with ID 10789 and 11806.

Acknowledgments This work was supported by grants from the ANR (HEMESTOCKEXCHANGE ANR-12-BSV3-0022-01 and LABEX DYNAMO ANR-11-LABEX-0011-01). We thank Nathalie Dautin for helpful suggestions and critical reading of the manuscript, as well as Andrew Thompson. We acknowledge Emmanuel Frachon and Christophe Thomas from the Institut Pasteur platform "Production of recombinant proteins" for large scale cultures used in this work, European Synchrotron Radiation Facility for the provision of time on the Titan Krios at beamline CM01, the Institut Pasteur Biological NMR Technological Platform for the use of the NMR spectrometers, the staff at the ESRF CM01 facility in Grenoble for help in the data collection, the staff at the Marseille proteomics facility and Djalila Djouadi and Diana Basto who initially contributed to this project. We thank M. Nilges for interest in this work and B. Miroux for constant support.

803
804

References

1. Noinaj N, Guillier M, Barnard TJ, Buchanan SK. 2010. TonB-dependent transporters: regulation, structure, and function. Annu Rev Microbiol 64:43-60.
2. Grinter R, Lithgow T. 2019. The structure of the bacterial iron-catecholate transporter Fiu suggests that it imports substrates via a two-step mechanism. J Biol Chem 294:19523-19534.
3. Cascales E, Lloubes R, Sturgis JN. 2001. The TolQ-TolR proteins energize TolA and share homologies with the flagellar motor proteins MotA-MotB. Mol Microbiol 42:795-807.
4. Braun V. 1989. The structurally related exbB and tolQ genes are interchangeable in conferring tonB-dependent colicin, bacteriophage, and albomycin sensitivity. J Bacteriol 171:6387-90.
5. Eick-Helmerich K, Braun V. 1989. Import of biopolymers into Escherichia coli: nucleotide sequences of the exbB and exbD genes are homologous to those of the tolQ and tolR genes, respectively. J Bacteriol 171:5117-26.
6. Braun V, Herrmann C. 1993. Evolutionary relationship of uptake systems for biopolymers in Escherichia coli: cross-complementation between the TonB-ExbB-ExbD and the TolA-TolQ-TolR proteins. Mol Microbiol 8:261-8.
7. Fischer E, Gunter K, Braun V. 1989. Involvement of ExbB and TonB in transport across the outer membrane of Escherichia coli: phenotypic complementation of exb mutants by overexpressed tonB and physical stabilization of TonB by ExbB. J Bacteriol 171:5127-34.
8. Ahmer BM, Thomas MG, Larsen RA, Postle K. 1995. Characterization of the exbBD operon of Escherichia coli and the role of ExbB and ExbD in TonB function and stability. J Bacteriol 177:4742-7.
9. Higgs PI, Myers PS, Postle K. 1998. Interactions in the TonB-dependent energy transduction complex: ExbB and ExbD form homomultimers. J Bacteriol 180:6031-8.
10. Braun V, Gaisser S, Herrmann C, Kampfenkel K, Killmann H, Traub I. 1996. Energy-coupled transport across the outer membrane of Escherichia coli: ExbB binds ExbD and TonB in vitro, and leucine 132 in the periplasmic region and aspartate 25 in the transmembrane region are important for ExbD activity. J Bacteriol 178:2836-45.
11. Gaisser S, Braun V. 1991. The tonB gene of Serratia marcescens: sequence, activity and partial complementation of Escherichia coli tonB mutants. Mol Microbiol 5:2777-87.
12. Paquelin A, Ghigo JM, Bertin S, Wandersman C. 2001. Characterization of HasB, a Serratia marcescens TonB-like protein specifically involved in the haemophore-dependent haem acquisition system. Mol Microbiol 42:995-1005.
13. Benevides-Matos N, Wandersman C, Biville F. 2008. HasB, the Serratia marcescens TonB paralog, is specific to HasR. J Bacteriol 190:21-7.
14. Celia H, Noinaj N, Zakharov SD, Bordignon E, Botos I, Santamaria M, Barnard TJ, Cramer WA, Lloubes R, Buchanan SK. 2016. Structural insight into the role of the Ton complex in energy transduction. Nature 538:60-65.
15. Maki-Yonekura S, Matsuoka R, Yamashita Y, Shimizu H, Tanaka M, Iwabuki F, Yonekura K. 2018. Hexameric and pentameric complexes of the ExbBD energizer in the Ton system. Elife 7.

851 16. Celia H, Botos I, Ni X, Fox T, De Val N, Lloubes R, Jiang J, Buchanan SK. 2019.
852 Cryo-EM structure of the bacterial Ton motor subcomplex ExbB–ExbD provides
853 information on structure and stoichiometry. Communications Biology 2:358.
854 17. Deme JC, Johnson S, Vickery O, Muellbauer A, Monkhouse H, Griffiths T, James
855 RH, Berks BC, Coulton JW, Stansfeld PJ, Lea SM. 2020. Structures of the stator
856 complex that drives rotation of the bacterial flagellum. Nat Microbiol 5:1553-1564.
857 18. Santiveri M, Roa-Eguiara A, Kuhne C, Wadhwa N, Hu H, Berg HC, Erhardt M,
858 Taylor NMI. 2020. Structure and Function of Stator Units of the Bacterial Flagellar
859 Motor. Cell 183:244-257 e16.
860 19. Altschul SF, Gish W, Miller W, Myers EW, Lipman DJ. 1990. Basic local alignment
861 search tool. J Mol Biol 215:403-10.
862 20. Ihsan MZ, Ahmad SJ, Shah ZH, Rehman HM, Aslam Z, Ahuja I, Bones AM, Ahmad
863 JN. 2017. Gene Mining for Proline Based Signaling Proteins in Cell Wall of
864 Arabidopsis thaliana. Front Plant Sci 8:233.
865 21. Mishra AK, Choi J, Moon E, Baek KH. 2018. Tryptophan-Rich and Proline-Rich
866 Antimicrobial Peptides. Molecules 23.
867 22. Ball LJ, Kühne R, Schneider-Mergener J, Oschkinat H. 2005. Recognition of proline-
868 rich motifs by protein-protein-interaction domains. Angew Chem Int Ed Engl
869 44:2852-69.
870 23. Marchler-Bauer A, Anderson JB, DeWeese-Scott C, Fedorova ND, Geer LY, He S,
871 Hurwitz DI, Jackson JD, Jacobs AR, Lanczycki CJ, Liebert CA, Liu C, Madej T,
872 Marchler GH, Mazumder R, Nikolskaya AN, Panchenko AR, Rao BS, Shoemaker
873 BA, Simonyan V, Song JS, Thiessen PA, Vasudevan S, Wang Y, Yamashita RA, Yin
874 JJ, Bryant SH. 2003. CDD: a curated Entrez database of conserved domain
875 alignments. Nucleic Acids Res 31:383-7.
876 24. Biville F, Cwerman H, Letoffe S, Rossi MS, Drouet V, Ghigo JM, Wandersman C.
877 2004. Haemophore-mediated signalling in Serratia marcescens: a new mode of
878 regulation for an extra cytoplasmic function (ECF) sigma factor involved in haem
879 acquisition. Mol Microbiol 53:1267-77.
880 25. Letoffe S, Delepelaire P, Wandersman C. 2004. Free and hemophore-bound heme
881 acquisitions through the outer membrane receptor HasR have different requirements
882 for the TonB-ExbB-ExbD complex. J Bacteriol 186:4067-74.
883 26. Aluyi HS, Boote V, Drucker DB, Wilson JM, Ling YH. 1992. Analysis of polar lipids
884 from some representative enterobacteria, Plesiomonas and Acinetobacter by fast atom
885 bombardment-mass spectrometry. J Appl Bacteriol 73:426-32.
886 27. Erdős G, Dosztányi Z. 2020. Analyzing Protein Disorder with IUPred2A. Curr Protoc
887 Bioinformatics 70:e99.
888 28. de Amorim GC, Prochnicka-Chalufour A, Delepelaire P, Lefevre J, Simenel C,
889 Wandersman C, Delepierre M, Izadi-Pruneyre N. 2013. The structure of HasB reveals
890 a new class of TonB protein fold. PLoS One 8:e58964.
891 29. Li H, Robertson AD, Jensen JH. 2005. Very fast empirical prediction and
892 rationalization of protein pKa values. Proteins 61:704-21.
893 30. Langsetmo K, Fuchs JA, Woodward C. 1991. The conserved, buried aspartic acid in
894 oxidized Escherichia coli thioredoxin has a pKa of 7.5. Its titration produces a related
895 shift in global stability. Biochemistry 30:7603-9.

896 31. Berka K, Hanák O, Sehnal D, Banás P, Navrátilová V, Jaiswal D, Ionescu CM,
897 Svobodová Vareková R, Koca J, Otyepka M. 2012. MOLEonline 2.0: interactive web-
898 based analysis of biomacromolecular channels. Nucleic Acids Res 40:W222-7.
899 32. Higgs PI, Larsen RA, Postle K. 2002. Quantification of known components of the
900 Escherichia coli TonB energy transduction system: TonB, ExbB, ExbD and FepA.
901 Mol Microbiol 44:271-81.
902 33. Ollis AA, Manning M, Held KG, Postle K. 2009. Cytoplasmic membrane
903 protonmotive force energizes periplasmic interactions between ExbD and TonB. Mol
904 Microbiol 73:466-81.
905 34. Garcia-Herrero A, Peacock RS, Howard SP, Vogel HJ. 2007. The solution structure of
906 the periplasmic domain of the TonB system ExbD protein reveals an unexpected
907 structural homology with siderophore-binding proteins. Mol Microbiol 66:872-89.
908 35. Ollis AA, Postle K. 2011. The same periplasmic ExbD residues mediate in vivo
909 interactions between ExbD homodimers and ExbD-TonB heterodimers. J Bacteriol
910 193:6852-63.
911 36. Klebba PE. 2016. ROSET Model of TonB Action in Gram-Negative Bacterial Iron
912 Acquisition. J Bacteriol 198:1013-21.
913 37. Boags AT, Samsudin F, Khalid S. 2019. Binding from Both Sides: TolR and Full-
914 Length OmpA Bind and Maintain the Local Structure of the E. coli Cell Wall.
915 Structure 27:713-724 e2.
916 38. Hickman SJ, Cooper REM, Bellucci L, Paci E, Brockwell DJ. 2017. Gating of TonB-
917 dependent transporters by substrate-specific forced remodelling. Nat Commun
918 8:14804.
919 39. Larsen RA, Thomas MG, Wood GE, Postle K. 1994. Partial suppression of an
920 Escherichia coli TonB transmembrane domain mutation (delta V17) by a missense
921 mutation in ExbB. Mol Microbiol 13:627-40.
922 40. Ollis AA, Kumar A, Postle K. 2012. The ExbD periplasmic domain contains distinct
923 functional regions for two stages in TonB energization. J Bacteriol 194:3069-77.
924 41. Kohler SD, Weber A, Howard SP, Welte W, Drescher M. 2010. The proline-rich
925 domain of TonB possesses an extended polyproline II-like conformation of sufficient
926 length to span the periplasm of Gram-negative bacteria. Protein Sci 19:625-30.
927 42. Létoffé S, Ghigo JM, Wandersman C. 1993. Identification of two components of the
928 Serratia marcescens metalloprotease transporter: protease SM secretion in Escherichia
929 coli is TolC dependent. J Bacteriol 175:7321-8.
930 43. Guzman LM, Belin D, Carson MJ, Beckwith J. 1995. Tight regulation, modulation,
931 and high-level expression by vectors containing the arabinose PBAD promoter. J
932 Bacteriol 177:4121-30.
933 44. Zheng SQ, Palovcak E, Armache JP, Verba KA, Cheng Y, Agard DA. 2017.
934 MotionCor2: anisotropic correction of beam-induced motion for improved cryo-
935 electron microscopy. Nat Methods 14:331-332.
936 45. Zhang K. 2016. Gctf: Real-time CTF determination and correction. J Struct Biol
937 193:1-12.
938 46. Gomez-Blanco J, de la Rosa-Trevin JM, Marabini R, Del Cano L, Jimenez A,
939 Martinez M, Melero R, Majtner T, Maluenda D, Mota J, Rancel Y, Ramirez-Aportela
940 E, Vilas JL, Carroni M, Fleischmann S, Lindahl E, Ashton AW, Basham M, Clare
941 DK, Savage K, Siebert CA, Sharov GG, Sorzano COS, Conesa P, Carazo JM. 2018.

Using Scipion for stream image processing at Cryo-EM facilities. J Struct Biol 204:457-463.

47. Zivanov J, Nakane T, Forsberg BO, Kimanius D, Hagen WJ, Lindahl E, Scheres SH. 2018. New tools for automated high-resolution cryo-EM structure determination in RELION-3. Elife 7.

48. Afonine PV, Poon BK, Read RJ, Sobolev OV, Terwilliger TC, Urzhumtsev A, Adams PD. 2018. Real-space refinement in PHENIX for cryo-EM and crystallography. Acta Crystallogr D Struct Biol 74:531-544.

49. Emsley P, Lohkamp B, Scott WG, Cowtan K. 2010. Features and development of Coot. Acta Crystallogr D Biol Crystallogr 66:486-501.

50. Moriarty NW, Grosse-Kunstleve RW, Adams PD. 2009. electronic Ligand Builder and Optimization Workbench (eLBOW): a tool for ligand coordinate and restraint generation. Acta Crystallogr D Biol Crystallogr 65:1074-80.

51. Punjani A, Rubinstein JL, Fleet DJ, Brubaker MA. 2017. cryoSPARC: algorithms for rapid unsupervised cryo-EM structure determination. Nat Methods 14:290-296.

52. Rohou A, Grigorieff N. 2015. CTFFIND4: Fast and accurate defocus estimation from electron micrographs. J Struct Biol 192:216-21.

53. Pettersen EF, Goddard TD, Huang CC, Couch GS, Greenblatt DM, Meng EC, Ferrin TE. 2004. UCSF Chimera--a visualization system for exploratory research and analysis. J Comput Chem 25:1605-12.

54. Lefevre J, Delepelaire P, Delepierre M, Izadi-Pruneyre N. 2008. Modulation by substrates of the interaction between the HasR outer membrane receptor and its specific TonB-like protein, HasB. J Mol Biol 378:840-51.

55. Delaglio F, Grzesiek S, Vuister GW, Zhu G, Pfeifer J, Bax A. 1995. NMRPipe: a multidimensional spectral processing system based on UNIX pipes. J Biomol NMR 6:277-93.

56. Vranken WF, Boucher W, Stevens TJ, Fogh RH, Pajon A, Llinas M, Ulrich EL, Markley JL, Ionides J, Laue ED. 2005. The CCPN data model for NMR spectroscopy: development of a software pipeline. Proteins 59:687-96.

57. Wishart DS, Bigam CG, Yao J, Abildgaard F, Dyson HJ, Oldfield E, Markley JL, Sykes BD. 1995. 1H, 13C and 15N chemical shift referencing in biomolecular NMR. J Biomol NMR 6:135-40.

58. Lefèvre J, Simenel C, Delepelaire P, Delepierre M, Izadi-Pruneyre N. 2007. (1)H, (13)C and (15)N resonance assignments of the C-terminal domain of HasB, a specific TonB like protein, from Serratia marcescens. Biomol NMR Assign 1:197-9.

979 **Tables**

Afipia broomeae	Hartmannibacter diazotrophicus	Phreatobacter stygius
Agrobacterium rhizogenes	Hoeflea olei	Phyllobacterium zundukense
Aliihoeflea sp.	Hyphomicrobium nitrativorans	Proteobacteria bacterium
Aminobacter aminovorans	Insolitispirillum peregrinum	Pseudaminobacter manganicus
Amorphus coralli	Kaistia granuli	Pseudochrobactrum asaccharolyticum
Ancylobacter aquaticus	Ketogulonicigenium robustum	Pseudolabrys taiwanensis
Aquamicrobium aerolatum	Labrys okinawensis	Pseudorhizobium pelagicum
Aurantimonas manganoxydans	Magnetospirillum gryphiswaldense	Pseudorhodoplanes sinuspersici
Aureimonas flava	Mangrovicella endophytica	Reyranella massiliensis
Azorhizobium caulinodans	Mesorhizobium loti	Rhizobium tropici
Azospirillum brasilense	Methylobrevis pamukkalensis	Rhodoligotrophos sp.
bacterium A52C2	Methylocapsa acidiphila	Rhodomicrobium udaipurense
Bartonella apis	Methyloceanibacter stevinii	Rhodopseudomonas pseudopalustris
Beijerinckiaceae bacterium	Methylocella silvestris	Rhodospirillum centenum
Blastochloris sp.	Methyloligella halotolerans	Rhodovarius sp.
Bosea vaviloviae	Methylopila sp.	Roseococcus sp.
Bradyrhizobium yuanmingense	Methylovirgula ligni	Roseospirillum parvum
Brucella sp.	Microvirga aerophila	Sinirhodobacter sp.
Chelatococcus asaccharovorans	Neorhizobium alkalisoli	Sinorhizobium sp.
Ciceribacter lividus	Nitratireductor pacificus	Skermanella aerolata
Devosia psychrophila	Nitrobacter hamburgensis	Sphingobium chlorophenolicum
Dongia mobilis	Nitrospirillum amazonense	Sphingomonas sp.
Enterovirga rhinocerotis	Niveispirillum cyanobacteriorum	Sphingopyxis sp.
Erythrobacter	Ochrobactrum thiophenivorans	Sphingorhabdus sp.
Falsochrobactrum ovis	Paenirhodobacter enshiensis	Starkeya novella
Geminicoccus roseus	Paracoccus aminovorans	Tardiphaga robiniae
Granulibacter bethesdensis	Paramesorhizobium deserti	Telmatospirillum siberiense
Haematobacter massiliensis	Parvibaculum lavamentivorans	Variibacter gotjawalensis
Hansschlegelia zhihuaiae	Phaeospirillum fulvum	Xanthobacter autotrophicus

980
981

982 Table I: a list of selected species of Alphaproteobacteria where “extralong” ExbB’s are found.

983 All those species also contain HasB orthologs, except for the ones in red.

984

Complex	**ExbB**	**ExbB-ExbD**
Deposition ID	EMD-10789, PDB 6YE4	EMD-11806, PDB ID 7AJQ
Data collection and processing		
Microscope type, camera	ESRF Titan Krios, Gatan K2	ESRF Titan Krios, Gatan K2
Magnification	165000	139000
Voltage (kV)	300	300
Electron exposure (e–/Å^2)	56	55
Defocus range (μm)	-1.5 to -2.5	-1 to -3
Pixel size (Å)	0.87	1.067
Initial particle images (no.)	850000	1373000
Final particle images (no.)	157000	158000
Map resolution (Å)	3.1	3.96
FSC threshold	0.143	0.143
Map resolution range (Å)	3.1-5.5	3.96-8
Symmetry imposed	C5	C1
Initial model used	Phyre2 homology model based on 5SV0	Our ExbB structure
Model composition		
Non-hydrogen atoms	9145	9256
Protein residues	1180	1229
Ligands	PGT : 5	0
B factors (Å^2)		
Protein min/max/mean	21.58/ 145.06/ 45.97	93.07/ 411.58/ 169.35
Ligand min/max/mean	45.43/ 46.91/ 46.12	
R.m.s. deviations		
Bond length (Å) (# >4σ)	0.026 (3)	0.003 (0)
Bond angles (°) (# > 4σ)	1.56 (8)	0.573 (4)
Validation		
Refined model CC	0.85	0.77
MolProbity score	1.1	2.03
Clashscore	3	15.3
Poor rotamers (%)	0	0
Ramachandran plot		
Favored (%)	99	95
Allowed (%)	1	5
Disallowed (%)	0	0

Table II: Data collection, processing, and refinement statistics for $ExbB_{Sm}$ and $ExbBD_{Sm}$.

989 Strains :
990 *E. coli* K12 C600
991 *E. coli* K12 C600Δ*hemA::Km*^{r}Δ*exbBD*
992 *E. coli* K12 C600Δ*hemA::Km*^{r}Δ*exbBD*Δ*tonB*
993 *E. coli* K12 XL1-Blue
994 *E. coli* K12 JP313
995 *E. coli* K12 JP313Δ*exbBD*Δ*tonB*
996 *E. coli* K12 C600Δ*exbBD*
997 *E. coli* BL21DE3
998 *S. marcescens* Db11
999
1000 Plasmids :
1001 pBAD24: lab collection
1002 pBAD33: lab collection
1003 pAM238: lab collection
1004 pAMHasISRADE: lab collection
1005 pAMHasISRADEB: this work
1006 pBADExbBD$_{Ec}$: this work
1007 pBADExbBD$_{Sm}$: this work
1008 pBADExbBD$_{Ec\text{-}Sm76\text{-}88}$: this work
1009 pBADExbBD$_{Ec\text{-}Sm76\text{-}84}$: this work
1010 pBADExbBD$_{Sm\text{-}Ec39\text{-}51}$: this work
1011 pBADExbBD$_{delextss}$: this work
1012 pBADHasB: lab collection
1013 pBADExbBD$_{Sm}$His6: this work
1014 pBADExbB$_{Sm}$His6: this work
1015 pBADExbB$_{Smdelextss}$His6: this work
1016
1017 Oligonucleotides:
1018 ExbBDSm5' 5'-GGAGGAATTCACCATGAAAACGGCTGGCAAGAAT -3'
1019 ExbBDSm3' 5'-AAGCTTGCATGCCTATTTGGCGGCGCCTTCCA-3'
1020 SphIHisCtexbDSm 5'-TTGCATGCCTAATGGTGATGGTGATGGTGTTTGGCGCGCCTTC-3'
1021 BglIIexbDSm 5'-GCGCTTAAATGAAGATCTGGACGACAGCGG-3'
1022 ExbBD5c 5'-CAGGAGGAATTCACCATGGGTAATAATTTAATGCAGACGGA-3'
1023 ExbBD3c 5'-AAGCTTGCATGCTTACTTCGCTTTGGCGGTTTCTT-3'
1024 PBADFOR 5'-CTGACGCTTTTTATCGCAAC-3'
1025 ExbBHis6 5'-
1026 AAGCTTGCATGCCTAATGGTGATGGTGATGGTGCCCCGCCCGCAGTTG-3'
1027 ExbBEcSm76-88.1 5'P-GGCAGTGAACTGCTGCGCGCCAAGCGTCGCCTTAAGCGCGAG-3'
1028 ExbBEcSm76-88.2 5'P-TTTAGCGAACAAAATGGTCCAGGTGACTACGGAGGCCAAAAT-3'
1029 ExbBEcSm76-84.1 5'P-CTAAAGGCAGTGAATTCTTCAATCAGAAGCGTCG-3'
1030 ExbBEcSm76-84.2 5'P-CGAACAAAATGGTCCAGGTGACTACGGAGGCCA-3'
1031 ExbBSmEc39-51.1 5'P-GCGTAGAGTTCTTCAATCAGAAGCGCCGTCTGCGTCGCGA-3'
1032 ExbBSmEc39-51.2 5'P-TCTTACTGAAGAAGATTGCCCAGGTCACGATAGACGCCAG-3'
1033 ExbBdelextss1 5'P- GAAACCCGCGGCATGGACCTGTCCATTTGGGG-3'
1034 ExbBdelextss2 5'P- TGCCTGCGCGCTGCCGGCCAGCCCCACAA-3'
1035
1036 Table III: list of strains, plasmids and oligonucleotide sequences used in this work
1037

1038 **Figure Legends**
1039
1040 Figure 1: ExbB sequence analysis. A: alignment of $ExbB_{Ec}$ (top) with $ExbB_{Sm}$ (bottom), made
1041 with DNA Strider v1.4x-2b, CEA. In red is shown the signal sequence from $ExbB_{Sm}$, and in
1042 blue the periplasmic extension, not present in $ExbB_{Ec}$. The consensus sequence is shown on
1043 the middle line, where + indicates similar amino-acid residues. B: Weblogo (24)
1044 representation of 131 « long » ExbB aminoacid sequences aligned with Clustal omega (25);
1045 those with much shorter periplasmic extensions have been excluded from the alignment. The
1046 orange boxes show the position of the three TM segments from the *E. coli* 5SV0 structure.
1047
1048
1049 Figure 2: $ExbBD_{Sm}$ complements $ExbBD_{Ec}$. overnight growth in LB broth of *E. coli*
1050 C600Δ*exbBD*(pBAD24) (blue), C600Δ*exbBD*(pBAD24$ExbBD_{Ec}$) (orange), and
1051 C600Δ*exbBD*(pBAD24$ExbBD_{Sm}$) (grey), without (0) or with 100 and 200µM iron chelator
1052 di-pyridyl (DiP). One representative experiment is shown. The vertical axis represents
1053 mDO_{600nm} absorbance units.
1054
1055 Figure 3: Role of HasB and TonB on bacterial growth. A: representation of the constructions
1056 used in Figure 3 B, 3C, 3D and elsewhere in this work. ss refers to the signal sequence, ext to
1057 the periplasmic extension of $ExbB_{Sm}$, and tm1, tm2 and tm3 to the first, second and third
1058 ExbB transmembrane segments, respectively. B and C: growth around wells of *E. coli*
1059 C600Δ*hemA*Δ*tonB*Δ*exbBD* harbouring pAMHasISRADEB and specified recombinant plasmids
1060 (B and C left parts) or *E. coli* C600Δ*hemA*Δ*exbBD* harbouring pAMHasISRADE and specified
1061 recombinant plasmids (B and C right parts); the pictures were taken after overnight growth at
1062 37°C (B), or after 36hrs growth (C). Arabinose concentration was 40µg/ml. Dipyridyl (DiP)
1063 iron chelator concentration was either 100 or 200µM. Heme-BSA concentrations inside the
1064 wells were 10, 2 and 0,4µM. D: growth curves in microplates of the same strains as in B/C;
1065 DiP concentration was 100µM, arabinose concentration 4µg/ml, Heme-BSA 1µM. Colored
1066 dots in B and C refer to the equivalent growth conditions in D.
1067
1068
1069 Figure 4: Homogeneity assessment of ExbB and ExbBD. Size exclusion chromatography
1070 profiles of representative purification of respectively $ExbB_{Sm}$His6 (A) and $ExbBD_{Sm}$His6 (B)
1071 on a Superose 6 10/300 column. The 280nm absorbance is plotted as a function of elution
1072 volume. A Coomassie-stained gel of the pooled peak fractions is shown on the right of each
1073 profile together with a molecular weight ladder on the right (respectively 15, 25, 35, 40, 55,
1074 70, 100, 130 and 170kDa). The faint band present in the Exb B_{Sm}His6 sample above 100kDa
1075 was identified as AcrB using mass spectrometry.
1076
1077 Figure 5:
1078 Interaction of $HasB_{CTD}$ with the periplasmic fragment of $ExbB_{Sm}$, as detected by NMR. A:
1079 Superposed $^{1}H–^{15}N$ HSQC spectra of 0.15 mM ^{15}N-labelled $HasB_{CTD}$ in 50mM sodium
1080 phosphate, pH 7, 50 mM NaCl in the presence (red) or absence (black) of the periplasmic
1081 peptide of $ExbB_{Sm}$ residues 1-44. B and C: $HasB_{CTD}$ residues (PDB code 2M2K) exhibiting the
1082 highest CSP in the presence of the periplasmic peptide of $ExbB_{sm}$ are coloured red (B: surface
1083 representation; C: cartoon representation). The residues showing the highest CSP are indicated.
1084

1085 Figure 6: ExbB TM1 interacts with HasB. A: bacterial growth curves of *E. coli*
1086 C600Δ*hemA*Δ*exbBD*Δ*tonB* harbouring pAMHasISRADEB plasmid together with either
1087 pBAD24 (medium-blue), pBADExbBD$_{Sm}$ (orange) or pBADExbBD$_{Smdelextss}$ (yellow),
1088 pBADExbBD$_{Ec}$ (grey), pBADExbBD$_{EcSm76-88}$ (green), pBADExbBD$_{EcSm76-84}$ (dark-blue),
1089 pBADExbBD$_{SmEc39-51}$ (magenta) in the presence of 1µM He-BSA as heme source, 4µg/ml
1090 arabinose to induce ExbBD expression and 100µM dipyridyl to induce iron starvation (see
1091 Materials and Methods for further details). The optical path was ca. 3mm long, and each
1092 curve represents the mean of four replicates of the same culture, recorded every 30 minutes
1093 for 66 hours. Bottom: Coomassie-blue stained gel (B) and immunodetection (C) with anti-
1094 His6 antibody of membrane preparations of *E. coli* C600 harbouring either pBAD24 plasmid
1095 (1), pBADExbB$_{Sm}$ (2) or pBADExbB$_{Smdelextss}$ (3). The equivalent of 0.6 OD$_{600nm}$ was loaded
1096 in B, and of 0.3 OD$_{600nm}$ in C.
1097
1098 Figure 7: Representation of the pentameric structure of ExbB$_{Sm}$ solved by cryo-EM. A: the
1099 cryo-EM density map is shown, each monomer with distinct colours, view from the side. The
1100 yellow/grey regions represent non-protein density. The yellow regions were modeled as PG
1101 molecules. B: view from the cytoplasmic side. C: superposition of a monomer of ExbB$_{Ec}$
1102 (dark grey) and ExbB$_{Sm}$ (red), represented as ribbon. The membrane thickness is represented
1103 by the dotted lines and the transmembrane segments TM1 (part of α2 helix), TM2 (part of α6
1104 helix) and TM3 (part of α7 helix) are indicated. D: close-up representation of one PG density;
1105 E: fitting of the PG molecule inside the density; nearby ExbB residues are depicted as sticks
1106 using the Coot software (49).
1107
1108 Figure 8: Structure of ExbBD$_{Sm}$ solved by cryo-EM. The same color code as in Figure 7 for is
1109 used the ExbB monomers and the two ExbD monomers are colored yellow and gold. A: side
1110 view; B: view from the periplasmic space. C: clipped side view, with the helix of each ExbD
1111 monomer represented (yellow and gold). For B and C, the insets show the clipping planes.
1112
1113 Figure 9: Visualisation of "tunnels" inside ExbBD structures from *S. marcescens* (A and C)
1114 and *E. coli* 6TYI structure (B and D), as calculated by the MoleOnline server with the same
1115 parameters. The Sm complex is colored as in Figure 8 and the Ec complex is coloured in
1116 shades of grey for ExbB and orange and red for ExbD. The tunnels are the green volumes
1117 running through the structure, viewed from the periplasmic space (A and B), and from the
1118 side (C and D). The average tunnel diameter is 3Å for *S. marcescens* and 2Å for *E. coli.*
1119
1120 Figure 10: ExbBD co-expression is necessary for HasB stabilisation. Immunodetection of
1121 HasB in whole cells of *E. coli* JP313Δ*exbBD*Δ*tonB*(pHasB33) also harbouring pBAD24
1122 (control), pBAD24ExbBD$_{Ec}$, pBAD24ExbBD$_{Sm}$ or pBAD24ExbBD$_{Ec-Sm76-88}$, in the presence
1123 of either glucose (1mg/ml) or arabinose (40µg/ml), indicated by the + signs. The equivalent of
1124 0.2OD$_{600nm}$ was loaded in each lane.
1125
1126 Figure 11: ExbB α2 helix: comparison between Sm and Ec. ExbB-ExbD structure with residues
1127 76-88 coloured black and showing the aminoacid side chains. A, general view of the Sm
1128 pentamer; B, an enlarged view of A; C and D, two perpendicular close-up views of the
1129 exchanged region 76-88 in Sm (C) and 39-51 in Ec (D). E and F: Helical wheel representations
1130 of the swapped regions between ExbB$_{Sm}$ and ExbB$_{Ec}$ TM1. E: ExbBSm 76-88; F: ExbBEc 39-
1131 51. The red boxes show the helical face in interaction with the membrane.

1132

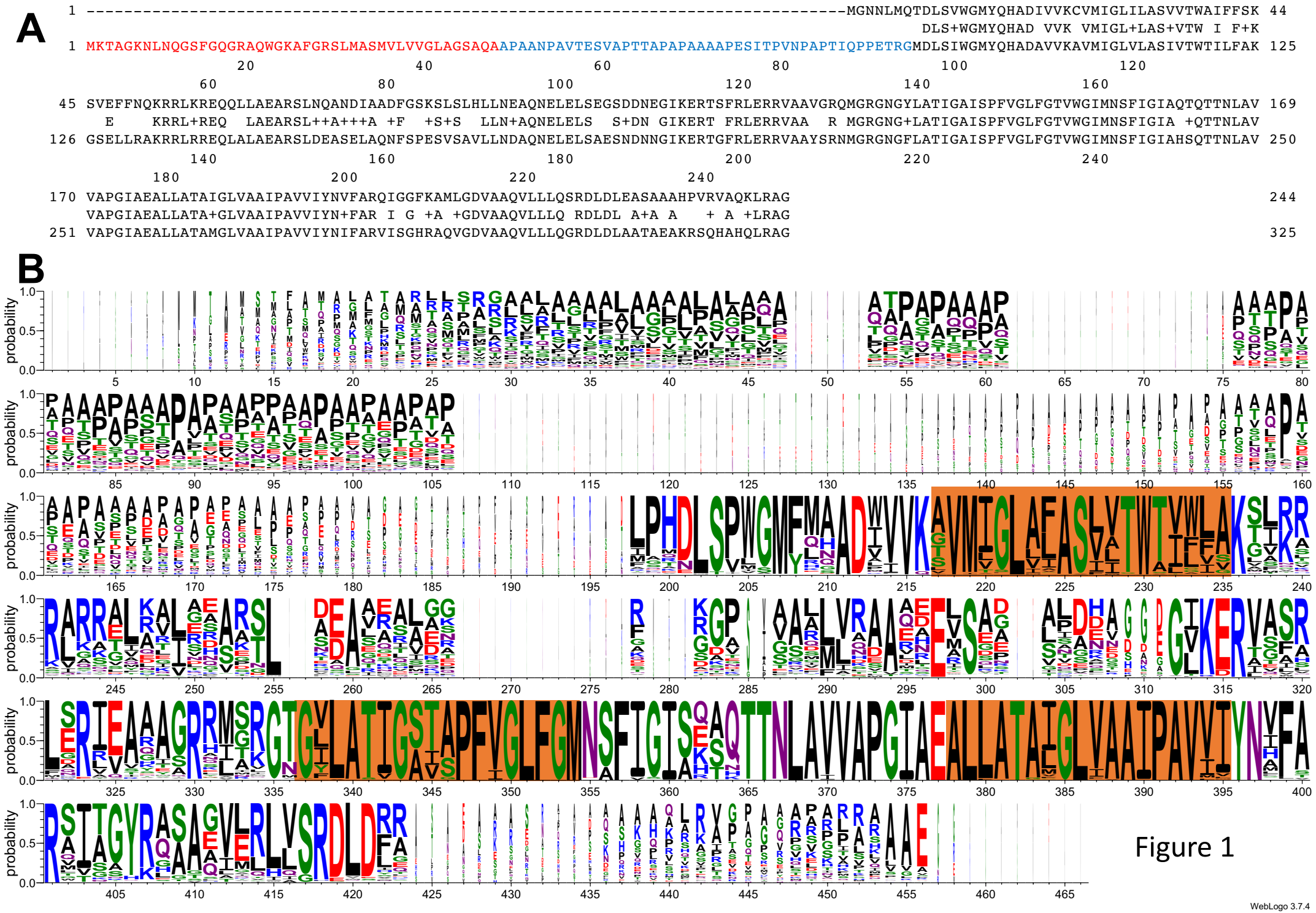
A
1 ----------MGNNLMQTDLSVWGMYQHADIVVKCVMIGLILASVVTWAIFFSK 44
DLS+WGMYQHAD VVK VMIGL+LAS+VTW I F+K
1 MKTAGKNLNQGSFGQGRAQWGKAFGRSLMASMVLVVGLAGSAQAAPAANPAVTESVAPTTAPAPAAAAPESITPVNPAPTIQPPETRGMDLSIWGMYQHADAVVKAVMIGLVLASIVTWTILFAK 125
20 40 60 80 100 120
60 80 100 120 140 160
45 SVEFFNQKRRLKREQQLLAEARSLNQANDIAADFGSKSLSLHLLNEAQNELELSEGSDDNEGIKERTSFRLERRVAAVGRQMGRGNGYLATIGAISPFVGLFGTVWGIMNSFIGIAQTQTTNLAV 169
E KRRL+REQ LAEARSL++A+++A +F +S+S LLN+AQNELELS S+DN GIKERT FRLERRVAA R MGRGNG+LATIGAISPFVGLFGTVWGIMNSFIGIA +QTTNLAV
126 GSELLRAKRRLRREQLALAEARSLDEASELAQNFSPESVSAVLLNDAQNELELSAESNDNNGIKERTGFRLERRVAAYSRNMGRGNGFLATIGAISPFVGLFGTVWGIMNSFIGIAHSQTTNLAV 250
140 160 180 200 220 240
180 200 220 240
170 VAPGIAEALLATAIGLVAAIPAVVIYNVFARQIGGFKAMLGDVAAQVLLLQSRDLDLEASAAAHPVRVAQKLRAG 244
VAPGIAEALLATA+GLVAAIPAVVIYN+FAR I G +A +GDVAAQVLLLQ RDLDL A+A A + A +LRAG
251 VAPGIAEALLATAMGLVAAIPAVVIYNIFARVISGHRAQVGDVAAQVLLLQGRDLDLAATAEAKRSQHAHQLRAG 325
B
probability
WebLogo 3.7.4

Figure 1

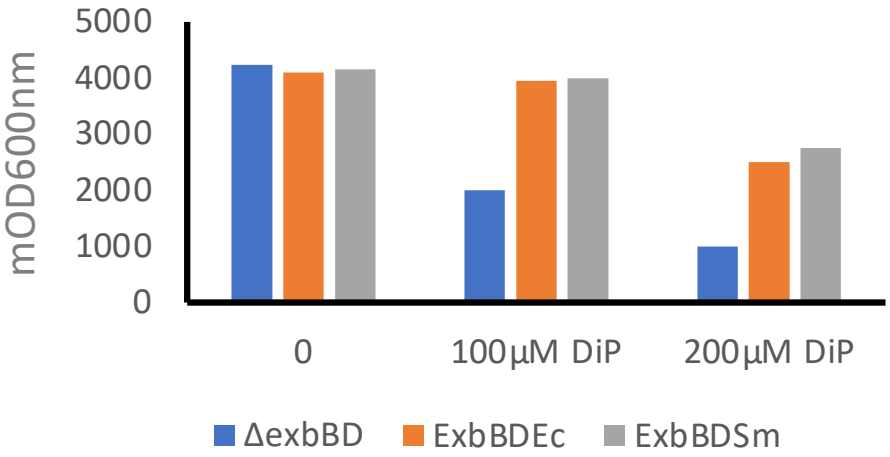
5000
4000
3000
2000
1000
0
mOD600nm
0
100µM DiP
200µM DiP
ΔexbBD
ExbBDEc
ExbBDSm

Figure 2

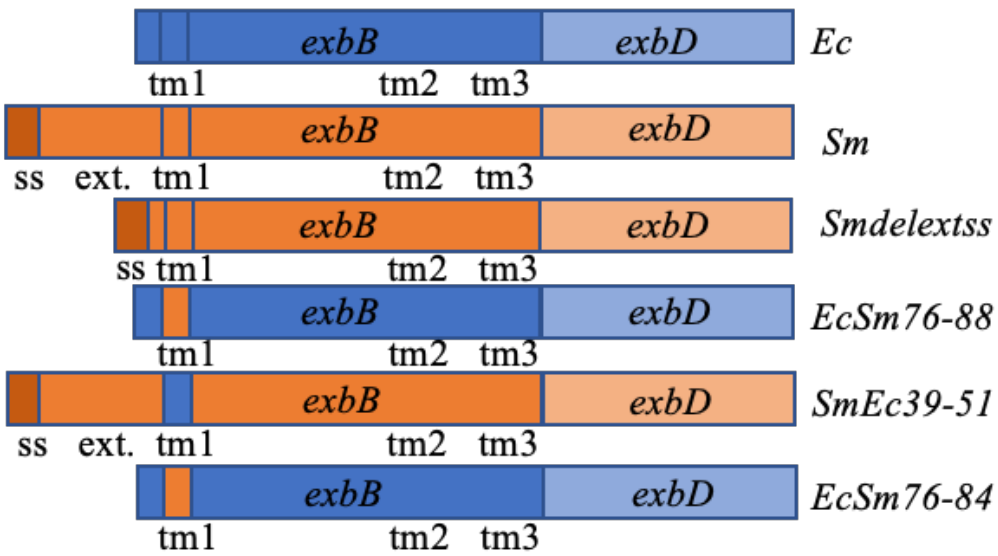
A
exbB
exbD
Ec
tm1
tm2
tm3
Sm
ss
ext.
Smdelextss
EcSm76-88
SmEc39-51
EcSm76-84

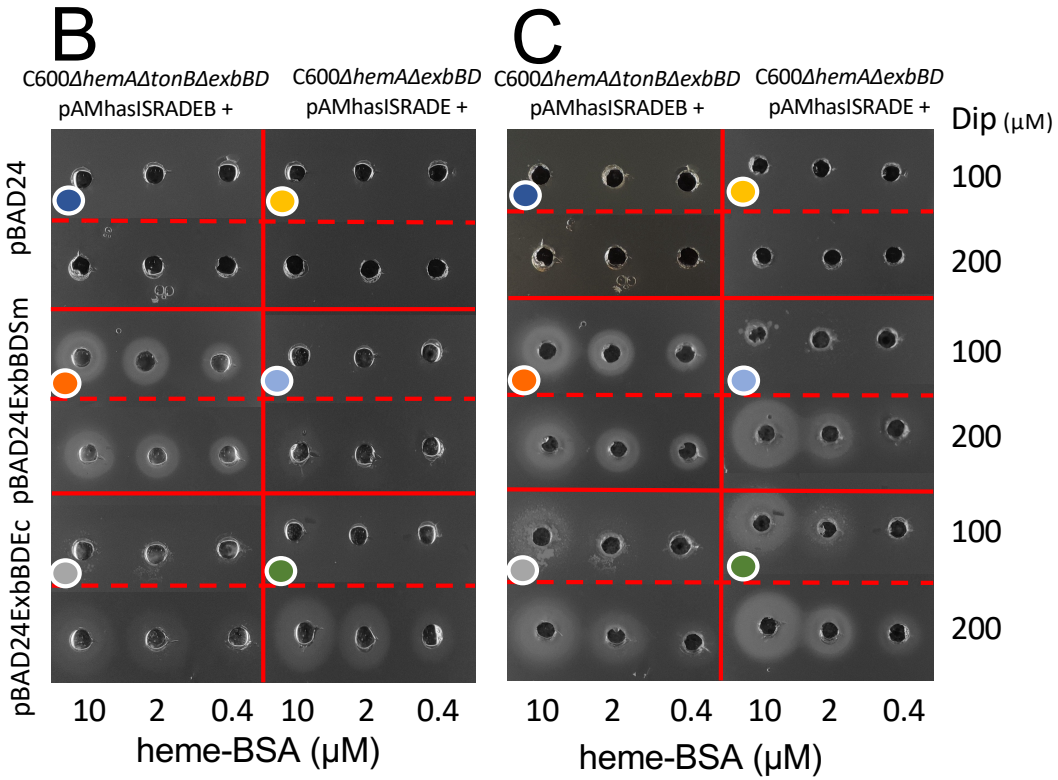
B
C
C600ΔhemAΔtonBΔexbBD pAMhasISRADEB +
C600ΔhemAΔexbBD pAMhasISRADE +
Dip (μM)
pBAD24
pBAD24ExbBDSm
pBAD24ExbBDEc
100
200
10
2
0.4
heme-BSA (μM)

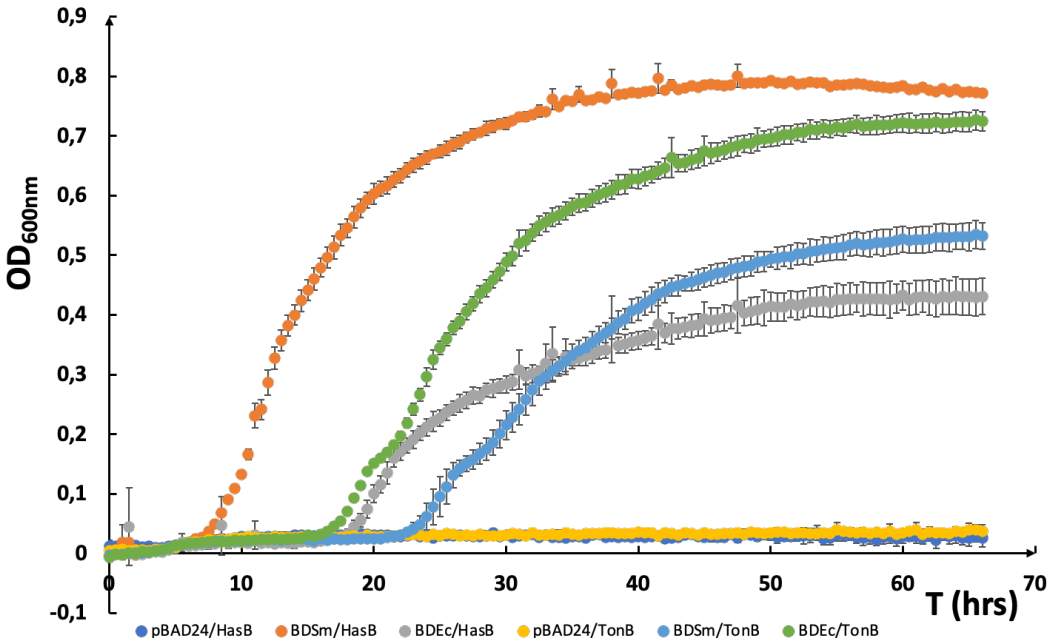
D
OD600nm
T (hrs)
pBAD24/HasB
BDSm/HasB
BDEc/HasB
pBAD24/TonB
BDSm/TonB
BDEc/TonB

Figure 3

A

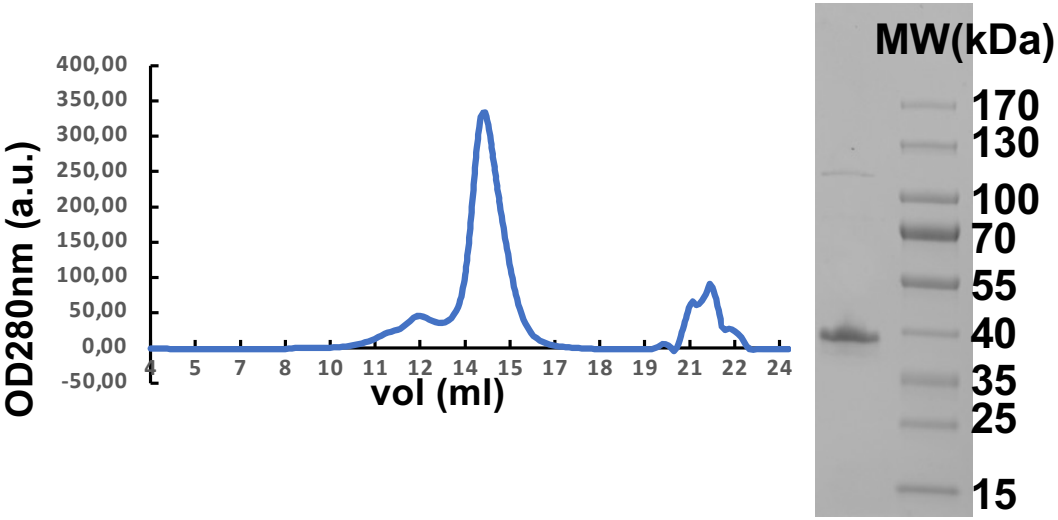
400,00
350,00
300,00
250,00
200,00
150,00
100,00
50,00
0,00
-50,00
OD280nm (a.u.)
4 5 7 8 10 11 12 14 15 17 18 19 21 22 24
vol (ml)
MW(kDa)
170
130
100
70
55
40
35
25
15

B

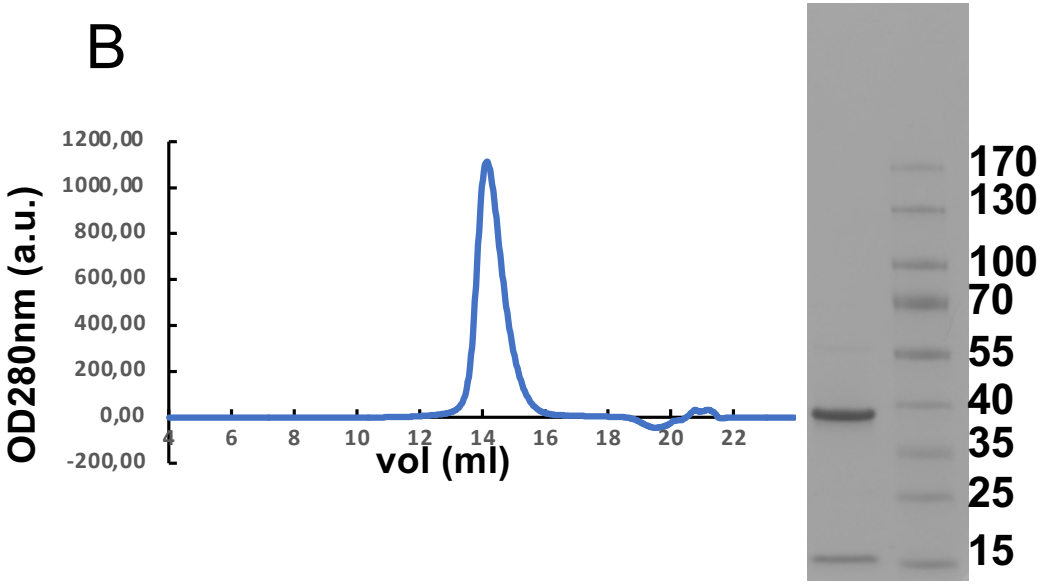
1200,00
1000,00
800,00
600,00
400,00
200,00
0,00
-200,00
OD280nm (a.u.)
4 6 8 10 12 14 16 18 20 22
vol (ml)
170
130
100
70
55
40
35
25
15

Figure 4

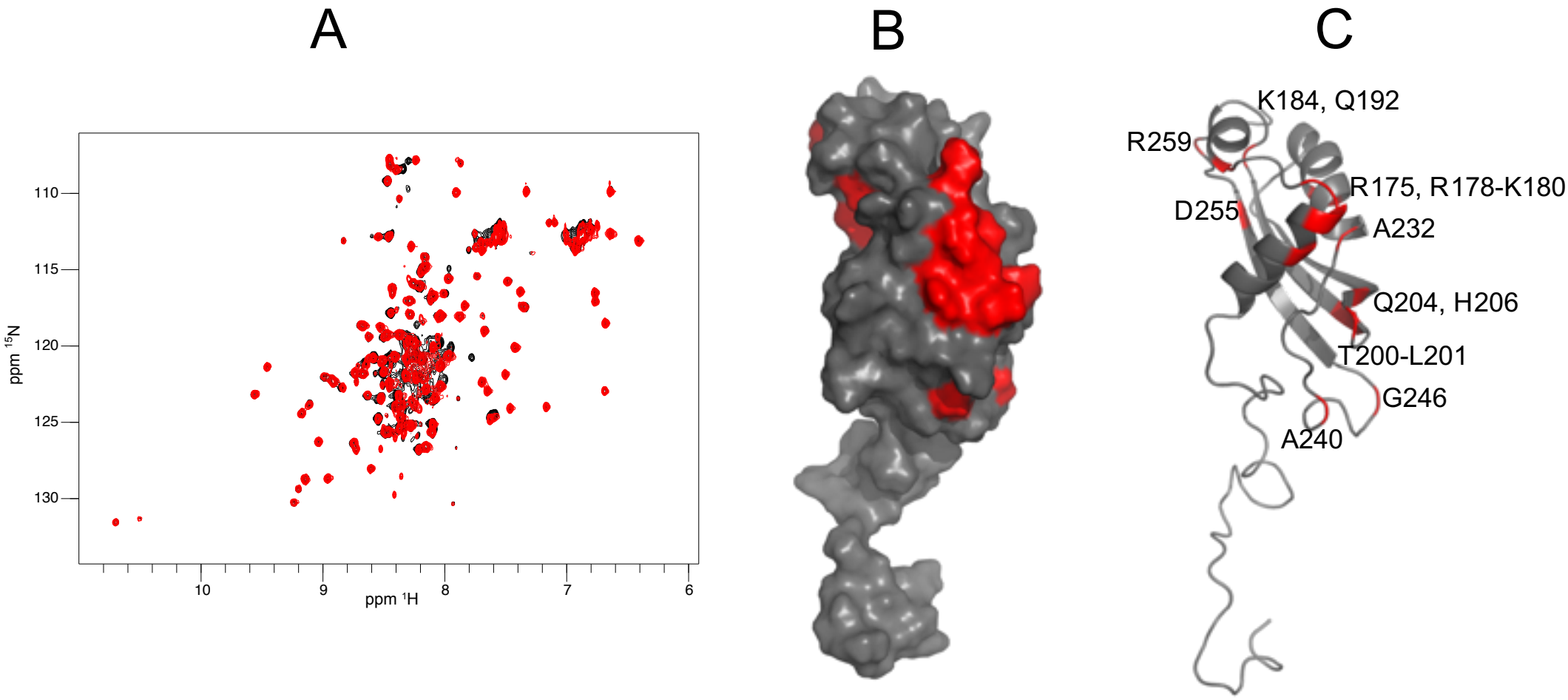
A
B
C
110
115
120
125
130
ppm 15N
10
9
8
7
6
ppm 1H
K184, Q192
R259
R175, R178-K180
D255
A232
Q204, H206
T200-L201
G246
A240

Figure 5

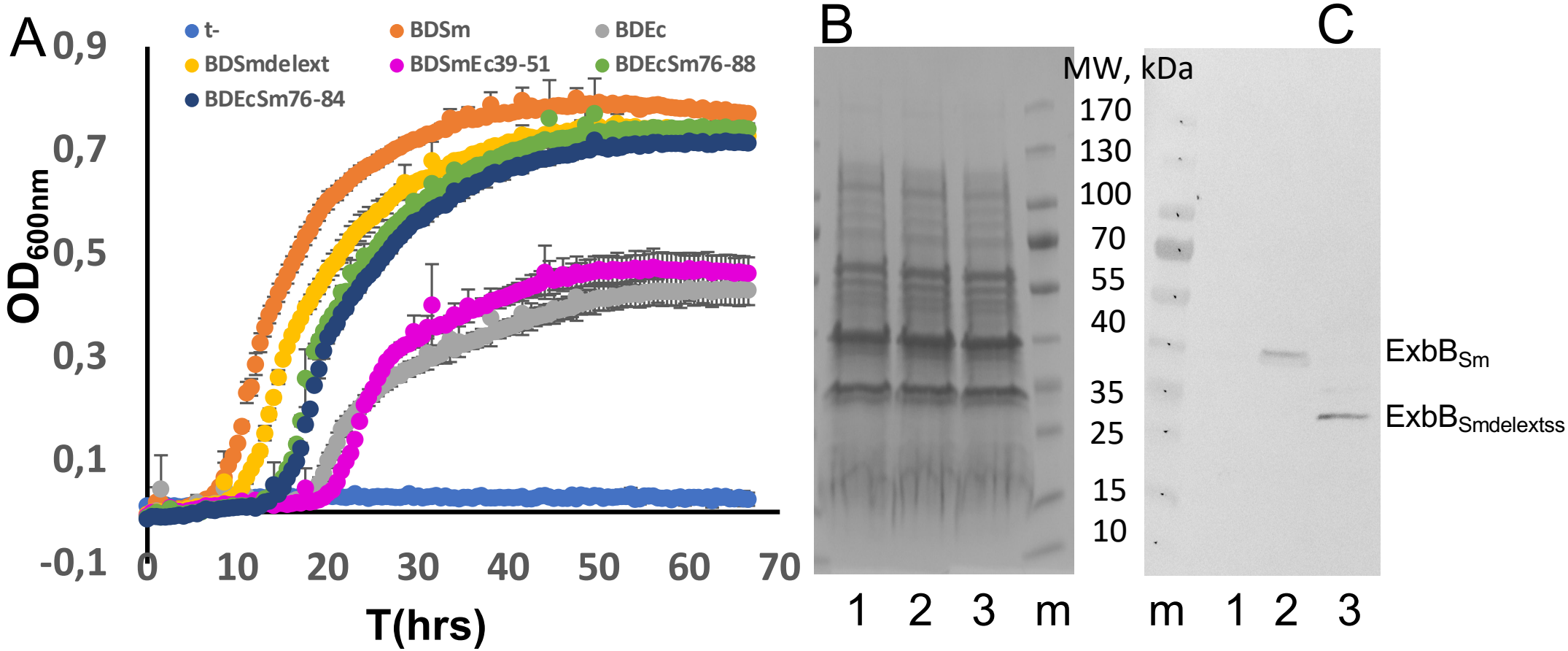
A
t-
BDSm
BDEc
BDSmdelext
BDSmEc39-51
BDEcSm76-88
BDEcSm76-84
OD600nm
0,9
0,7
0,5
0,3
0,1
-0,1
0
10
20
30
40
50
60
70
T(hrs)
B
C
MW, kDa
170
130
100
70
55
40
35
25
15
10
ExbBSm
ExbBSmdelextss
1
2
3
m
m
1
2
3

Figure 6

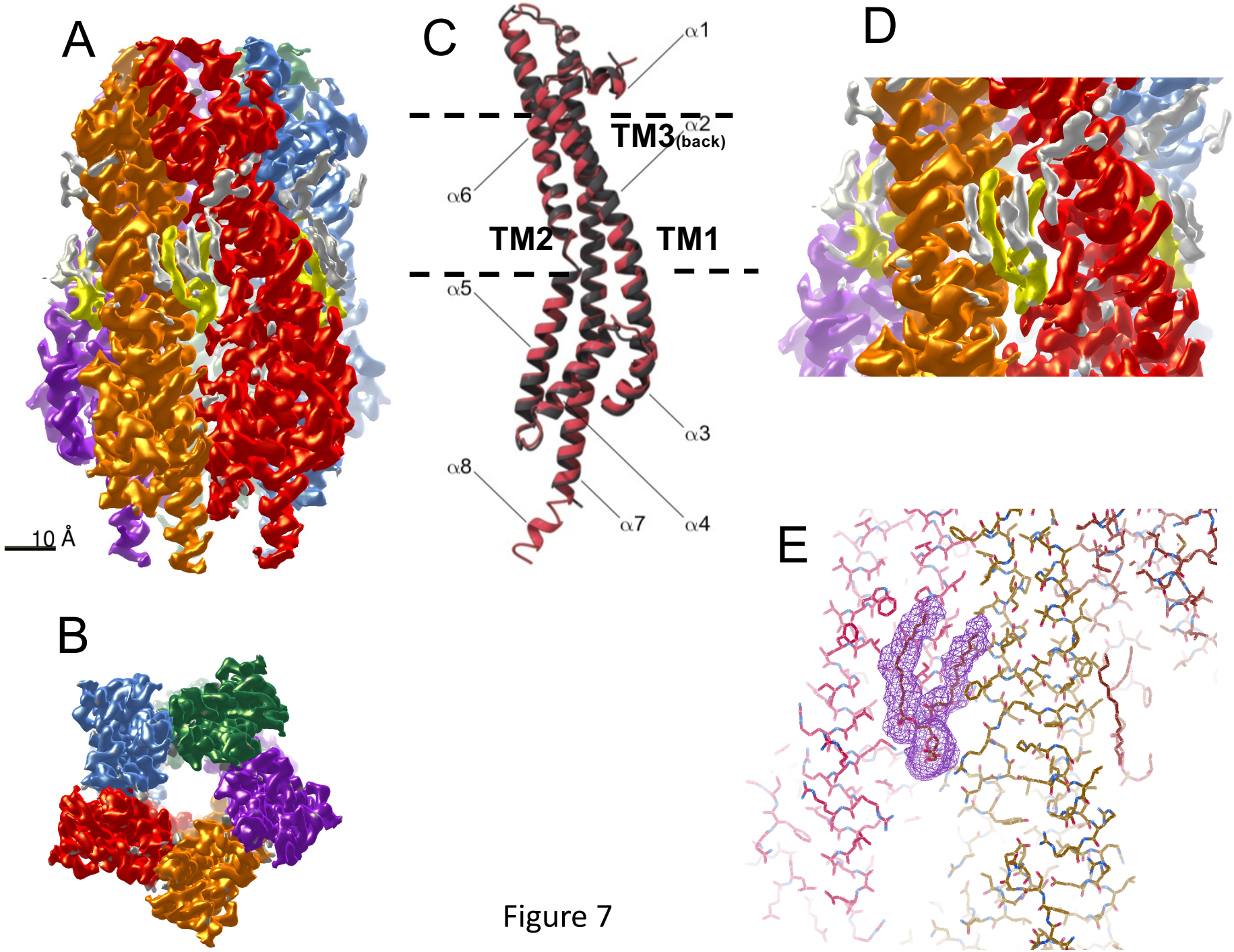

Figure 7

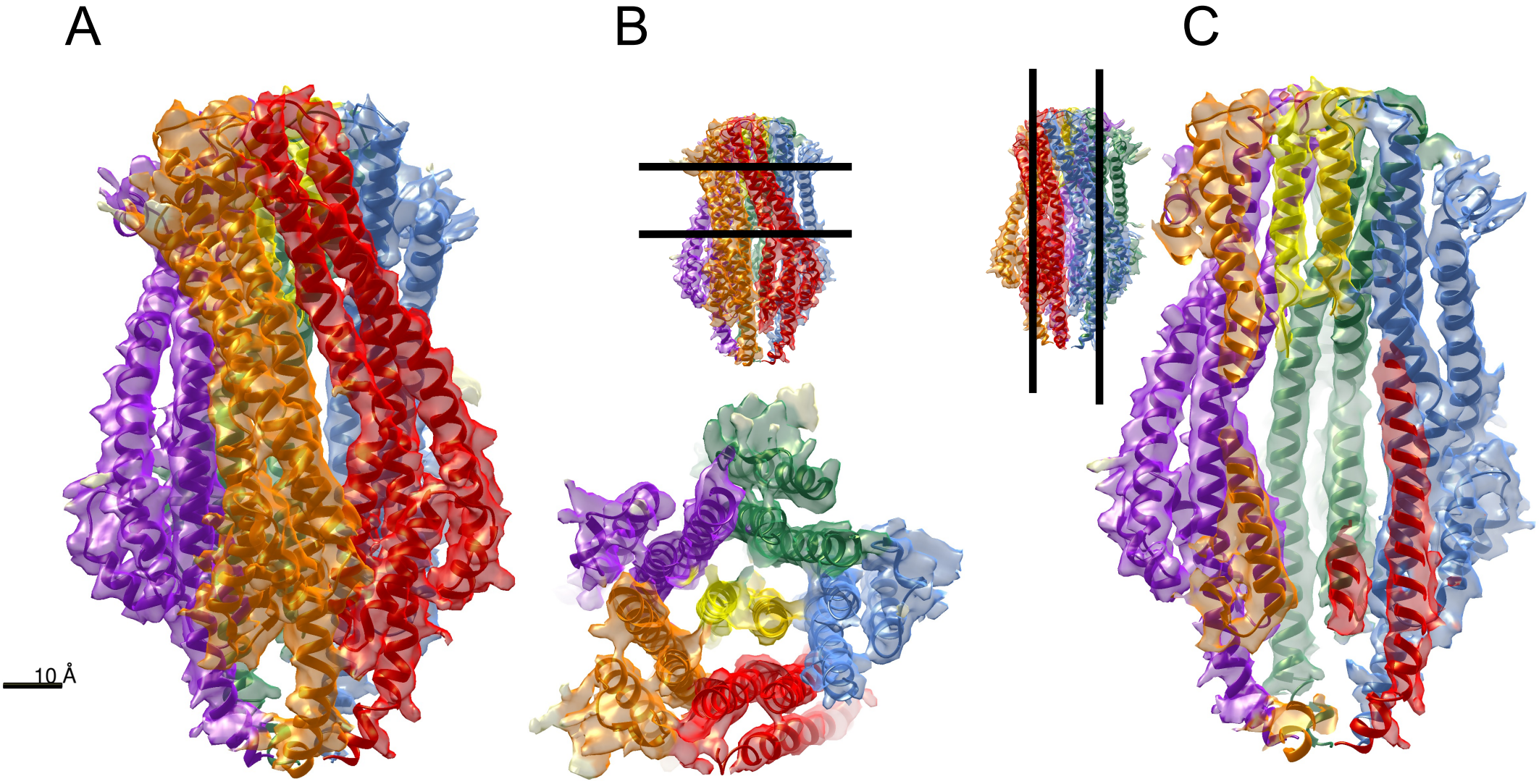

Figure 8

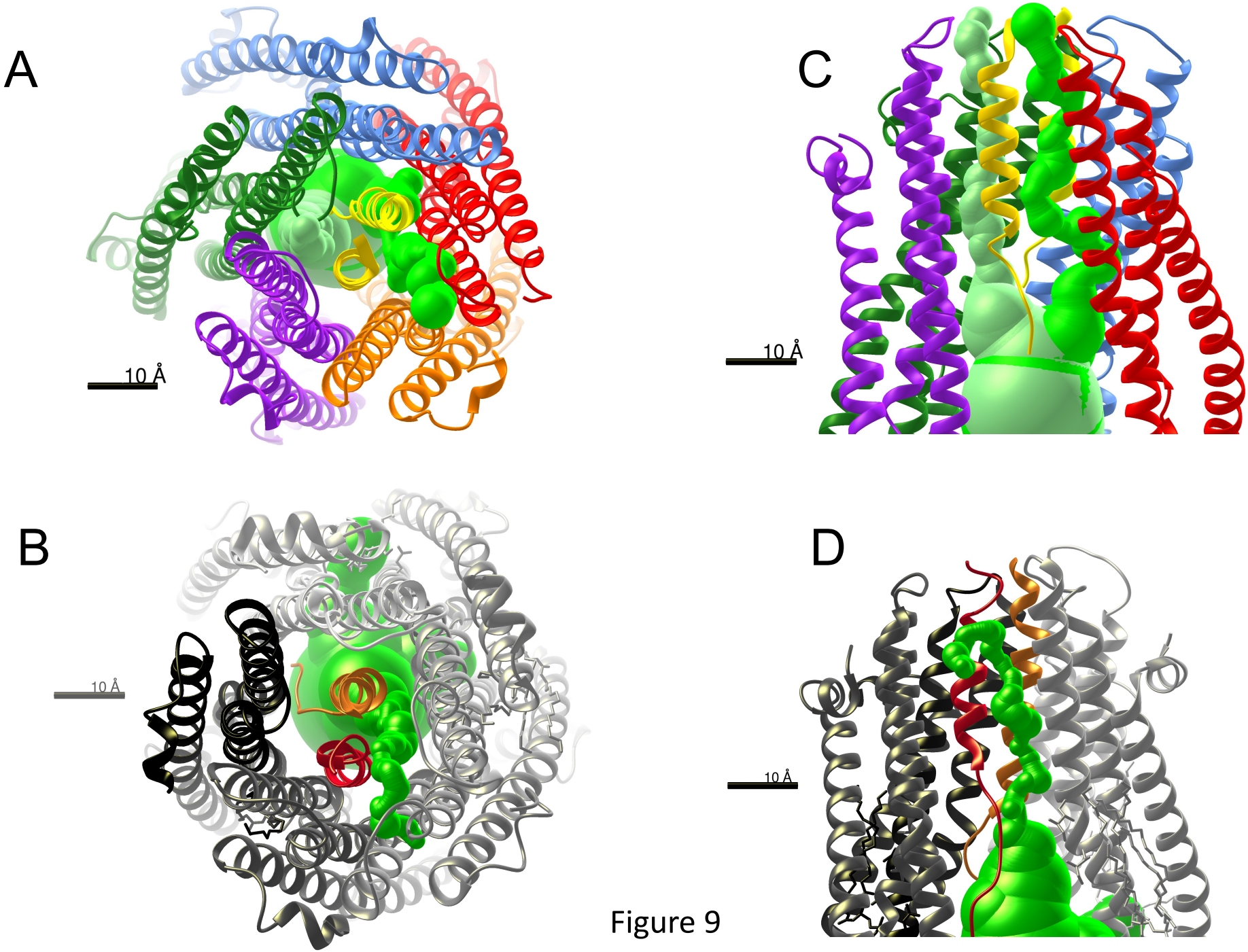

Figure 9

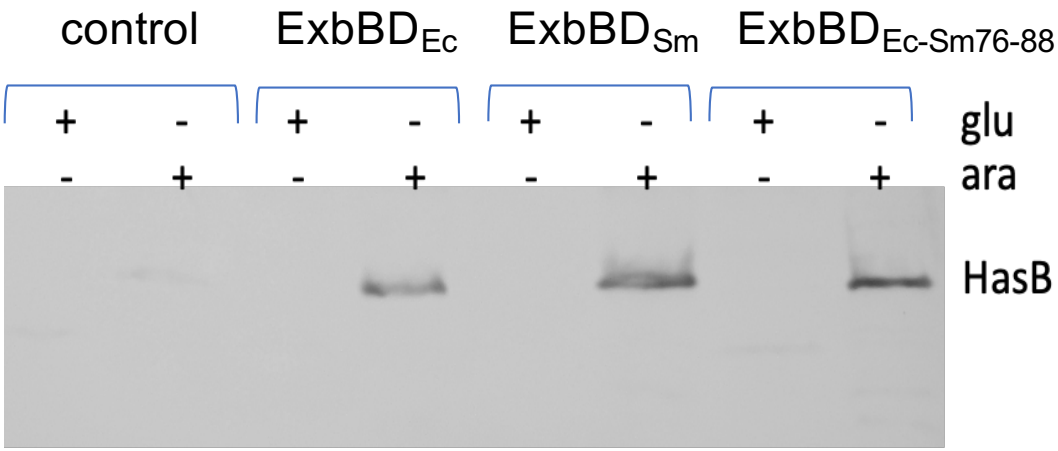
control
ExbBD$_{Ec}$
ExbBD$_{Sm}$
ExbBD$_{Ec\text{-}Sm76\text{-}88}$
+ - + - + - + -
glu
- + - + - + - +
ara
HasB

Figure 10

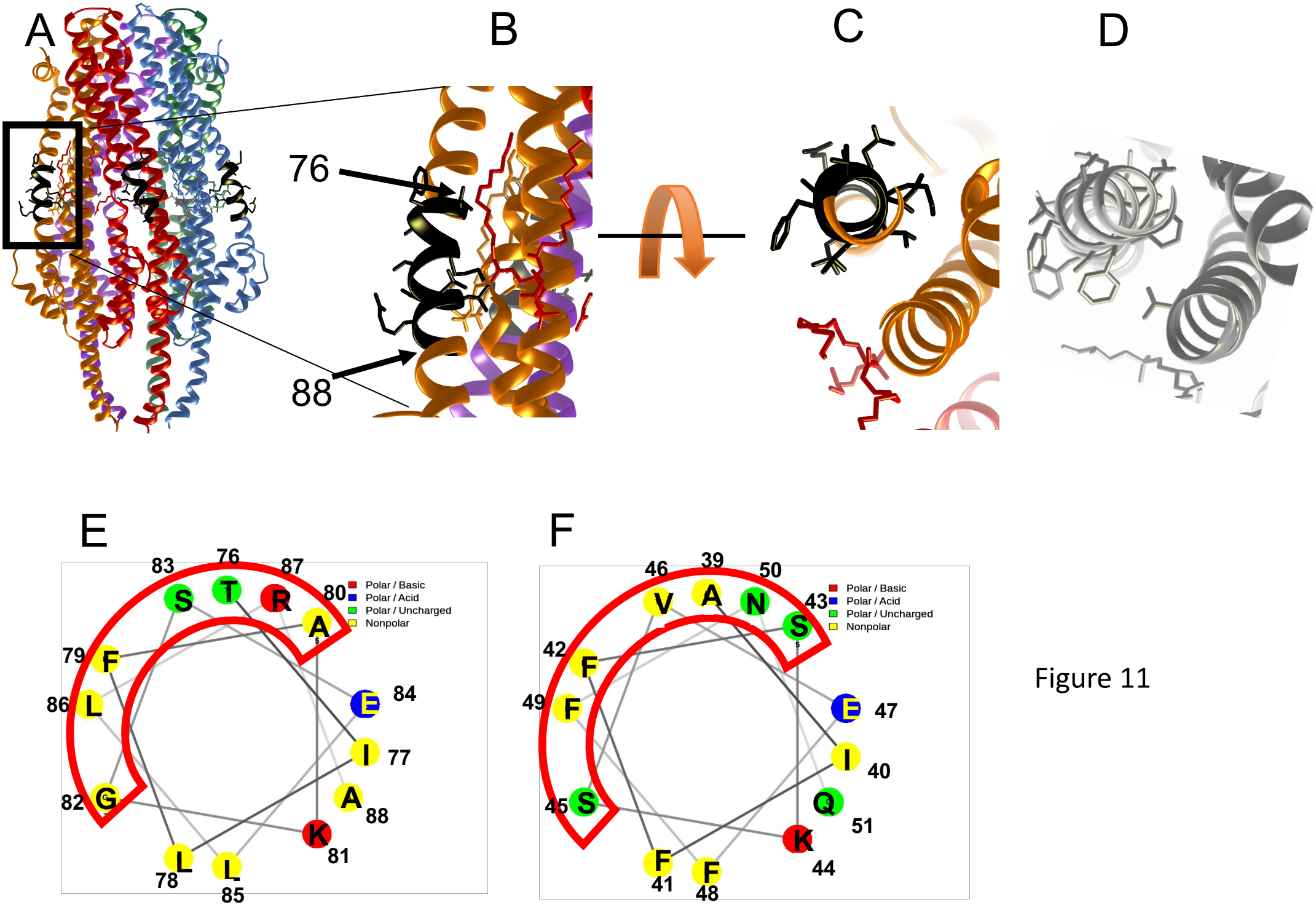
A
B
C
D
76
88
E
F
Polar / Basic
Polar / Acid
Polar / Uncharged
Nonpolar
83
76
87
80
79
86
84
77
82
88
81
78
85
46
39
50
43
42
49
47
40
45
51
44
41
48

Figure 11